

Origin of the Structure of the Kuiper Belt during a Dynamical Instability in the Orbits of Uranus and Neptune

Harold F. Levison

Southwest Research Institute, USA

Alessandro Morbidelli

Observatoire de la Côte d'Azur, France

Christa Van Laerhoven

Department of Physics and Astronomy, University of British Columbia

Rodney Gomes

Observatório Nacional/MCT, Brazil

and

Kleomenis Tsiganis

Department of Physics, Aristotle University of Thessaloniki, Greece

Received _____; accepted _____

ABSTRACT

We explore the origin and orbital evolution of the Kuiper belt in the framework of a recent model of the dynamical evolution of the giant planets, sometimes known as the *Nice* model. This model is characterized by a short, but violent, instability phase, during which the planets were on large eccentricity orbits. It successfully explains, for the first time, the current orbital architecture of the giant planets (Tsiganis et al. 2005), the existence of the Trojans populations of Jupiter and Neptune (Morbidelli et al. 2005), and the origin of the late heavy bombardment of the terrestrial planets (Gomes et al. 2005). One characteristic of this model is that the proto-planetary disk must have been truncated at roughly 30 to 35 AU so that Neptune would stop migrating at its currently observed location. As a result, the Kuiper belt would have initially been empty.

In this paper we present a new dynamical mechanism which can deliver objects from the region interior to ~ 35 AU to the Kuiper belt without excessive inclination excitation. In particular, we show that during the phase when Neptune’s eccentricity is large, the region interior to its 1:2 mean motion resonance becomes unstable and disk particles can diffuse into this area. In addition, we perform numerical simulations where the planets are forced to evolve using fictitious analytic forces, in a way consistent with the direct N-body simulations of the Nice model. Assuming that the last encounter with Uranus delivered Neptune onto a low-inclination orbit with a semi-major axis of ~ 27 AU and an eccentricity of ~ 0.3 , and that subsequently Neptune’s eccentricity damped in ~ 1 My, our simulations reproduce the main observed properties of the Kuiper belt at an unprecedented level. In particular, our results explain, at least qualitatively: 1) the so-existence of resonant and non-resonant populations, 2) the eccentricity–inclination distribution of the Plutinos, 3) the peculiar semi-major

axis – eccentricity distribution in the classical belt, 4) the outer edge at the 1:2 mean motion resonance with Neptune, 5) the bi-modal inclination distribution of the classical population, 6) the correlations between inclination and physical properties in the classical Kuiper belt, the existence of the so-called extended scattered disk. Nevertheless, we observe in the simulations a deficit of nearly-circular objects in the classical Kuiper belt.

1. Introduction

The Kuiper belt is the relic of the primordial planetesimal disk, shaped by various dynamical and collisional processes that occurred when the Solar System was evolving towards its present structure. Thus, studying the origin of the structure of the Kuiper belt is important because it can unveil the history of the formation and evolution of the giant planets and, more in general, of the proto-Solar System.

The main properties of the Kuiper belt that require an explanation in the framework of the primordial evolution of the Solar System are: (The following list is presented in no particular order.)

- i) The existence of conspicuous populations of objects in the main mean motion resonances (MMRs) with Neptune (2:3, 3:5, 4:7, 1:2, 2:5, etc.). Resonant objects form obvious vertical structures in a semi-major axis (a) versus eccentricity (e) plot, for example, see Fig. 1A. The resonant objects represent a significant fraction of the total trans-neptunian population. Trujillo et al. (2001) estimate that roughly 10% of the total population of the Kuiper belt are in the resonances, while Kavelaars et al. (2007) put the fraction of objects in Neptune’s 2:3 MMR alone at $\sim 20\%$.
- ii) The excitation of the eccentricities in the classical belt, which we define as the

collection of stable, non-resonant objects with $a < 48$ AU. The median eccentricity of the classical belt is ~ 0.07 . This value is small, but nevertheless it is an order of magnitude larger than what must have existed when the Kuiper belt objects (KBOs) formed (Stern & Colwell 1997a; Kenyon & Luu 1998 1999a; 1999b). It should be noted, however, that the upper eccentricity boundary of this population (see Fig. 1A) is set by the long-term orbital stability in this region (Duncan et al. 1995), and thus the classical belt could have originally contained objects with much larger eccentricities.

- iii) The a – e distribution of classical belt objects (see Fig. 1A) shows another distinct feature that models must explain. The population of objects on nearly-circular orbits effectively ‘ends’ at about 44 AU, and beyond this location the eccentricity tends to increase with semi-major axis (see Kavelaars et al. 2007 for a discussion). The lower bound of the bulk of the a – e distribution in the 44–48 AU range follows a curve that is steeper than a curve of constant q . Given that the observational biases are roughly a function of q , the apparent relative under-density of objects at low eccentricity in the region immediately interior to Neptune’s 1:2 MMR is likely to be a real feature of the Kuiper belt distribution.
- iv) The outer edge of the classical belt (Fig. 1A). This edge appears to be precisely at the location of the 1:2 MMR with Neptune. Again, the under density (or absence) of low eccentricity objects beyond the 1:2 MMR cannot be explained by observational biases (Trujillo & Brown 2001; Allen et al. 2001, 2002).
- v) The inclination distribution in the classical belt. Fig. 1B shows a cluster of objects with $i \lesssim 4^\circ$, but also several objects with much larger inclinations, up to $i \sim 30^\circ$. Observational biases definitely enhance the low inclination cluster relative to the large inclination population (the probability of discovery of an object in an ecliptic

survey is roughly proportional to $1/\sin(i)$). However, the cluster persists even when the biases are taken into account. Brown (2001) argued that the de-biased inclination distribution is bi-modal and can be fitted with two Gaussian functions, one with a standard deviation $\sigma \sim 2^\circ$ for the low-inclination core, and the other with $\sigma \sim 12^\circ$ for the high inclination population. Since the work of Brown, the classical population with $i < 4^\circ$ is called ‘cold population’, and the higher inclination classical population is called ‘hot population’. It is interesting to note that the fact that most known classical belt objects are members of the cold population is a result of observational biases. The hot population actually dominates in total number.

vi) The correlations between physical properties and orbital distribution. The cluster of low inclination objects visible in the (a, i) distribution disappears if one selects only objects with absolute magnitude $H \lesssim 6$ (Levison & Stern 2001). This implies that intrinsically bright objects are under represented in the cold population. Grundy et al. (2005) have shown that the objects of the cold population have a larger albedo, on average, than those of the hot population. Thus, the correlation found by Levison and Stern implies that the hot population contains bigger objects. Bernstein et al. (2004) showed that the hot population has a shallower H distribution than the cold population, which is consistent with the absence of the largest objects in the cold belt.

In addition, there is a well known correlation between color and inclination (Tegler & Romanishin 2000; Doressoundiram et al. 2001; Trujillo & Brown 2002; Doressoundiram et al. 2005; Elliot et al. 2005). The hot population objects show a wide range of colors, from red to gray. Conversely, the cold population objects are mostly red. In other words, the cold population shows a significant deficit of gray color bodies relative to the hot population. The same is true for the objects with $q > 39$ AU (Doressoundiram

et al. 2005). These objects are all red, regardless of their inclination. If one includes also objects with smaller q , then a correlation between color and perihelion distance becomes apparent (gray color objects becoming more abundant at low q).

- vii) The existence of the *extended scattered disk*, which consists of stable non-resonant objects with semi-major axes beyond Neptune’s 1:2MMR and mainly have perihelion distances between ~ 30 and ~ 40 AU. These objects have also been called *detached objects*. They cannot have been placed on their current orbits by the current configuration of the planets and thus supply an important constraint for formation models. It is important to note that we do not consider Sedna to be a member of the extended scattered disk. We believe that this object represents a totally different population that had a different origin (Mordibelli & Levison 2004; Kenyon & Bromley 2004a; Brasser et al. 2007).

- viii) The mass deficit of the Kuiper belt. The current mass of the Kuiper belt is very small — estimates range from $0.01 M_{\oplus}$ (Bernstein et al. 2004) to $0.1 M_{\oplus}$ (Gladman et al. 2001). The uncertainty is due mainly to the conversion from absolute magnitudes to sizes, assumptions about bulk density, and ambiguities in the size distribution. Whatever the exact mass really is, there appears to be a significant mass deficit (of 2–3 orders of magnitude) with respect to what models say was needed in order for the KBOs to accrete where we see them. In particular, the growth of these objects within a reasonable time (10^7 – 10^8 My) requires the existence of about 10 to $30 M_{\oplus}$ of solid material in a dynamically cold disk (Stern, 1996; Stern & Colwell, 1997a, 1997b; Kenyon & Luu, 1998; 1999a; 1999b; Kenyon & Bromley 2004b).

A good model of the Kuiper belt’s primordial evolution should explain all the properties detailed above. In the simplest scenario, the main features of the belt are the consequence of the outward migration of Neptune, due to its interaction with the primordial planetesimal

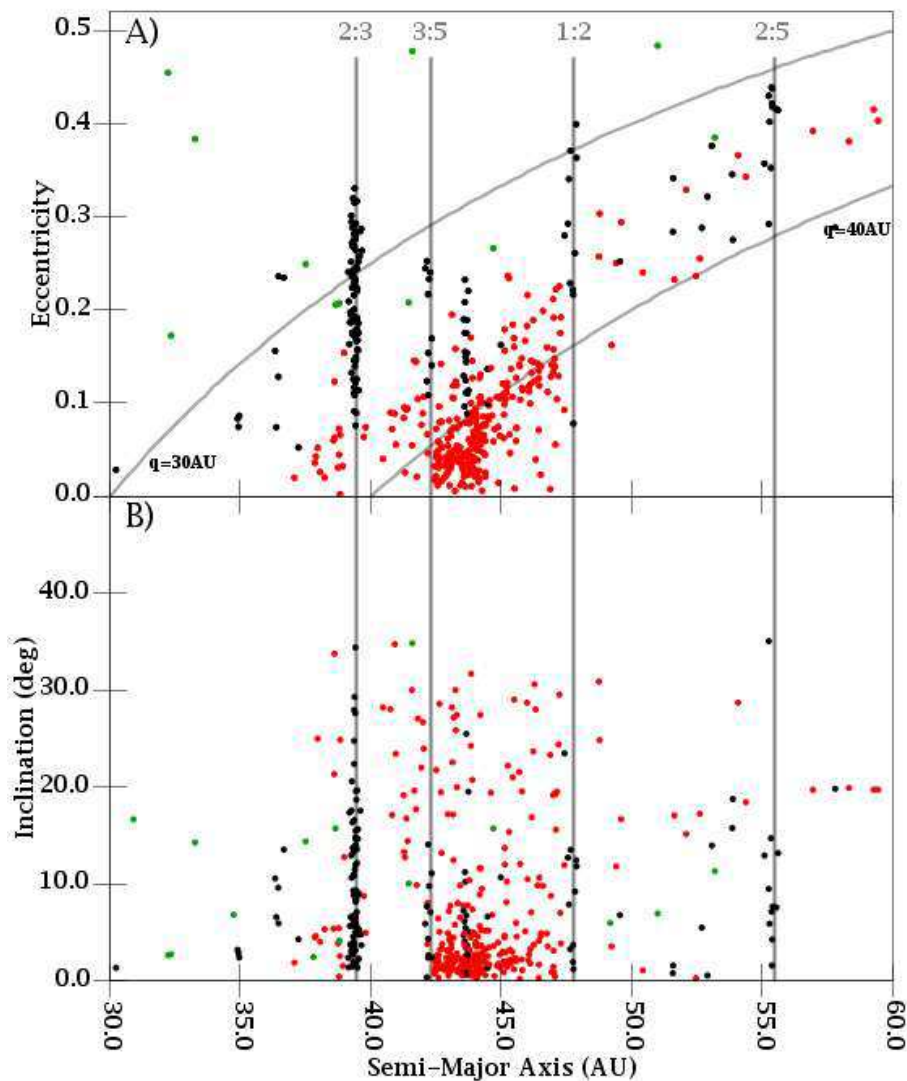


Fig. 1.— Observed orbital elements distribution of the (KBOs) with orbits determined from observations over at least three oppositions. We have employed the methods in Gladman et al. (2007) to classify these objects according to their dynamical behavior. In particular, the dots that are black represent objects in one of Neptune’s mean motion resonances, dots that are green are objects undergoing encounters with Neptune, and the red dots are non-resonant stable objects. A) Eccentricity versus semi-major axis. The two curves correspond to $q = 30$ AU and $q = 40$. B) semi-major axis versus inclination.

disk. In this scenario, the planetesimal disk, which was initially dynamically cold, extended to at least ~ 50 AU. Neptune migrated on a nearly-circular, low-inclination orbit, from an unconstrained initial location (estimates ranging from 18 AU — Gomes 2003 — to 23 AU — Malhotra 1995) up to its current orbital radius of 30 AU.

According to the above scenario, three main events happen in the Kuiper belt during this time. The main mean motion resonances with the Neptune, which moved along with the planet, captured objects from the cold distant disk that they swept through (Malhotra 1993, 1995; Hahn & Malhotra 1999, 2005). Simultaneously, a large fraction of the objects initially in the region swept by Neptune’s motion were scattered by the planet onto orbits with large eccentricity and semi-major axis. The relic of this population is now called the *scattered disk*. Finally, a small fraction of the scattered disk objects decoupled from the planet, decreasing their eccentricities through interactions with some secular or mean-motion resonances (Gomes 2003). If Neptune were not migrating, the decoupled objects would soon, once again, have evolved back onto Neptune-crossing orbits, because the dynamics are time reversible. However, Neptune’s migration broke the reversibility, and some of the decoupled bodies could manage to escape from the resonances and remained permanently trapped in the Kuiper belt. Gomes showed that the majority of these trapped bodies have large inclinations (acquired during the scattering phase), and identified them with the current hot Kuiper belt population. Some scattered disk bodies could also be trapped in the main MMR with Neptune (Gomes 2003), and mixed with those captured from the cold disk to form the current resonant populations.

Thus, in this view both the resonant populations and the hot population are the product of Neptune’s migration, whereas the cold population is the local, original Kuiper belt population which was only marginally perturbed during the resonance sweeping. Assuming that the physical properties of the bodies (colors and maximal sizes) varied in

the primordial disk with heliocentric distance, this scenario qualitatively explains why the scattered objects and hot classical belt objects — which mostly come from regions inside ~ 30 AU — appear to have similar color and size distributions, while the cold classical objects — the only ones that actually formed in the trans-Neptunian region — have different distributions.

Nevertheless, this scenario does not explain why the cold Kuiper belt did not retain its primordial mass, nor why its outer edge coincides with the location of Neptune’s 1:2 MMR. To solve these problems, Levison & Morbidelli (2003) proposed that the original planetesimal disk, in which the planets and KBOs formed, was truncated near 30 AU, and *all* the KBOs that we see were implanted in the Kuiper belt during Neptune’s migration. This idea also has the advantage of explaining why Neptune stopped migrating at 30 AU — it hit the edge of the disk (Gomes et al. 2004). In Levison & Morbidelli’s scenario, the Kuiper belt’s cold population was pushed outward from interior to 30 AU with the following mechanism. When Neptune was close enough to the Sun for its 1:2 MMR to be within the planetesimal disk, disk particles were trapped in this resonance as Neptune migrated (Malhotra 1995). As the resonance left the disk, it pushed the particles outward along with it. As these objects were driven from the Sun many had small eccentricities because of a newly discovered secular interaction with Neptune and they were progressively released from the resonance due to the non-smoothness of the planet’s migration. The 1:2 MMR does not excite inclinations, so that these bodies could retain their initial low inclinations during this process (hence the cold belt is cold). Another strength of this scenario is that the final edge of the cold belt naturally coincides with the final (and thus current) position of the 1:2 MMR. The low mass of the cold population is explained by the low efficiency of the transport/implantation process.

In the light of Gomes (2003) and Levison & Morbidelli (2003), the most important

properties of the Kuiper belt seem to be explained, at least qualitatively. Therefore, is there any need to re-investigate the problem? We think that the answer is yes, for at least three reasons. First, the idea that both the cold and the hot populations formed closer to the Sun and were transported outward re-opens the issue of the correlation between physical properties and final orbital distribution. Second, a quantitative comparison between the observed orbital distribution of the Kuiper belt and that expected from the sculpting model (including observational biases) has never been done. Third, and most importantly, our view of the evolution of the giant planets’ orbits has changed radically.

Last year, we proposed a new comprehensive scenario — now often called ‘the Nice model’ because we were all working in the city of Nice when the model was developed — that reproduces, for the first time, many of the characteristics of the outer Solar System. It quantitatively recreates the orbital architecture of the giant planet system (orbital separations, eccentricities, inclinations; Tsiganis et al. 2005) and the capture of the Trojan populations of Jupiter (Morbidelli et al. 2005) and Neptune (Tsiganis et al. 2005; Sheppard & Trujillo 2006) and many of the irregular satellites (Nesvorný et al. 2006). It also naturally supplies a trigger for the so-called Late Heavy Bombardment (LHB) of the terrestrial planets that occurred ~ 3.8 billion years ago (Tera et al. 1974), and quantitatively reproduces most of the LHB’s characteristics (Gomes et al. 2005). The evolution of the giant planets in the Nice model is substantially different from the smooth migration on low eccentricity, low inclination orbits, envisioned in Malhotra (1995), Gomes (2003), and Levison & Morbidelli (2003). Consequently, it is important to re-examine, from scratch, the issue of the primordial shaping of the Kuiper belt in the framework of the Nice model. This study could bring additional support, or refutation, of the Nice model, thus deepening our understanding of the processes at work in the early Solar System.

This paper is structured as follows. In section 2, we review the Nice model, stressing

the aspects that may be important for the structure of the Kuiper belt. In section 3 we discuss a new mechanism that could be effective for the transport of objects from the primordial planetesimal disk into the Kuiper belt region. The remaining part of the paper presents the results of our simulations. Section 4 focuses on the resulting a - e and i -distributions. Section 5 addresses the origin of the correlations between the physical and the orbital properties. Section 6 discusses several important issues such as: the efficiency of the overall transport mechanism and the origin of the mass deficit of the Kuiper belt (sect. 6.1); the orbital distribution of the Plutinos (sect. 6.2); and the filling of mean motion resonances beyond 50 AU (sect. 6.3). Section 7 summarizes the main results, stressing advantages and weak points of our model.

2. The ‘Nice’ model of evolution of the giant planets

The initial conditions of the Nice model are intended to represent the state of the outer Solar System at the time of disappearance of the gas disk. The giant planets are assumed to be initially on nearly-circular and coplanar orbits, consistent with the expectations from the theory of formation of giant planets (Pollack et al. 1996; Lubow et al. 1999). A pre-migration configuration is assumed, with planetary orbital separations that are significantly smaller than those currently observed. More precisely, the giant planet system is assumed to be in the range from ~ 5.5 AU to ~ 14 AU. The gas giants (Jupiter and Saturn) are placed closer to the Sun than the ice giants (Uranus and Neptune). Saturn is assumed to be closer to Jupiter than their mutual 1:2 MMR, a condition required in order to avoid a substantial amount of migration (Type II) during the gas disk lifetime (Masset & Snellgrove 2001; Morbidelli & Crida 2007). Overall, such a compact system is consistent with the constraints on the formation timescales of Uranus and Neptune (Levison & Stewart 2001; Thommes et al. 2003).

A planetesimal disk is assumed to exist beyond the orbits of the giant planets. In particular, it was assumed that particles inhabited only those regions where the dynamical lifetime of the individual objects is of the order of the gas disk lifetime (~ 3 My; see for example, Haisch, Lada & Lada 2001), or longer, because the planetesimals initially on orbits with shorter dynamical lifetimes should have been eliminated during the nebula era. This sets the inner edge of the disk to be about 1.5 AU beyond the location of the outermost planet. The outer edge of the disk is assumed at ~ 34 AU. It was found that in order to most accurately reproduce the characteristics of the outer planetary system the total mass of the disk must have been $\sim 35M_{\oplus}$.

With the above configuration, the planetesimals in the inner regions of the disk acquire planet-scattering orbits on a timescale of a few million years. Consequently, the migration of the giant planets proceeds at very slow rate, governed by the slow planetesimal escape rate from the disk (Fig. 2A). After a significant period of time, ranging from 60 My to 1.1 Gy in the simulations in Gomes et al. (2005), Jupiter and Saturn eventually cross their mutual 1:2 mean-motion resonance. (The upper range of this time-span is consistent with the timing of the LHB, which occurred approximately 650 My after planet formation.) The resonance crossing excites their eccentricities to values slightly larger than those currently observed.

The small jump in Jupiter’s and Saturn’s eccentricities drives up the eccentricities of Uranus and Neptune to the point where they start to approach each other. Thus, a short phase of violent encounters follows the resonance-crossing event (from ~ 878 to ~ 885 Myr in the example shown in Fig. 2). Consequently, both ice giants are scattered outward, onto large eccentricity orbits ($e \sim 0.25$ – 0.4) that penetrate deeply into the disk. This destabilizes the full planetesimal disk and disk particles are scattered all over the Solar System. The eccentricities of Uranus and Neptune and, to a lesser extent, of Jupiter and

Saturn, are damped on a timescale of a few My due to the dynamical friction exerted by the planetesimals. In the example shown in Fig. 2, Neptune’s eccentricity evolves from a peak of 0.22 to less than 0.05 in 2.4 Myr. Tsiganis et al. (2005) found that this damping time is between ~ 0.3 and ~ 4 Myr.

As a result of the gravitational influence of the disk, the planets decouple from each other, and the phase of mutual encounters rapidly ends. During and after the eccentricity damping phase, the giant planets continue their radial migration, and eventually reach final orbits when most of the disk has been eliminated (Fig. 2A). The final outcomes of the simulations of the Nice model reproduce quantitatively the current architecture of the giant planets, in terms of semi-major axes, eccentricities, and inclinations (Tsiganis et al. 2005).

The sudden destabilization of the planetesimal disk produces an abrupt spike in the flux of bodies from the outer Solar System entering the region of the terrestrial planets. In addition, the rapid migration of Jupiter and Saturn from their mutual 1:2 MMR to their current position, destabilizes approximately 90% of the asteroids residing in the asteroid belt at the time. Together, outer Solar System planetesimals and escaping asteroids cause a short-lived bombardment on the terrestrial planets lasting $\lesssim 100$ My — the magnitude of which is consistent with constraints on the lunar crater rate at ~ 3.8 Ga (Gomes et al. 2005).

Moreover, a fraction of the disk planetesimals are trapped onto Jovian Trojan orbits as Jupiter and Saturn migrate away from the 1:2 MMR. The orbital distribution of the trapped Trojans and their total mass is remarkably similar with the observed distribution and the total estimated population (Morbidelli et al. 2005). Neptune’s Trojans are also captured during the giant planet evolution, over a broad range of inclinations (Tsiganis et al. 2005), consistent with the inclination distribution of the newly discovered objects (although these are only 4 known objects; Trujillo & Sheppard 2006). Finally, disk particles can be captured into orbit around Saturn, Uranus, and Neptune during planet-planet encounters, thereby

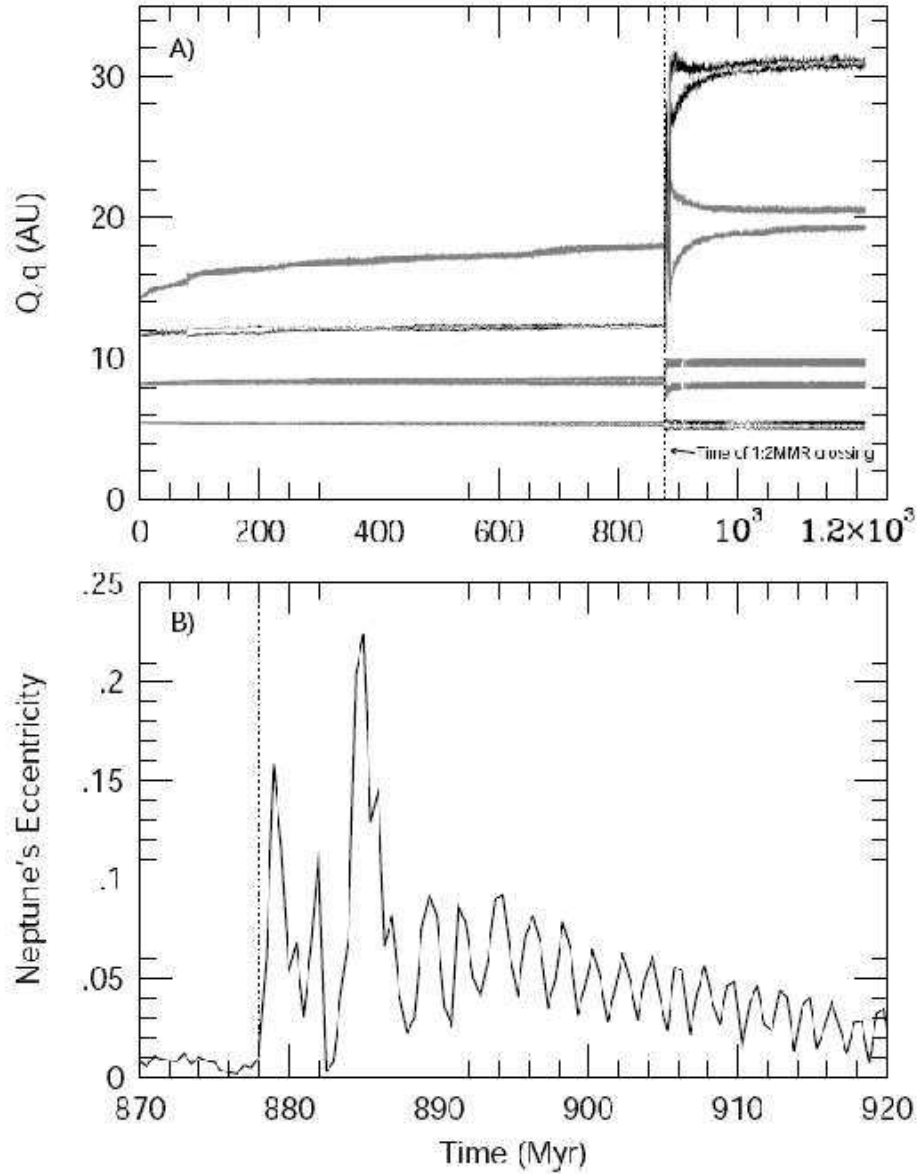


Fig. 2.— Giant planet evolution in the Nice model. A) Each planet is represented by a pair of curves – the top and bottom curves are the aphelion and perihelion distances, respectively. In this simulation Jupiter and Saturn cross their 1:2 mean-motion resonance at 878 My, which is indicated by the dotted line (From Gomes et al. 2005). B) The eccentricity of Neptune.

creating at least some of the observed irregular satellites (Nesvorný et al. 2006).

The unprecedented success of the Nice model calls for a re-investigation of the formation of the Kuiper belt. An essential ingredient of the model is that, at least at the time of the LHB, the planetesimal disk was truncated at 30–35 AU, otherwise Neptune would have migrated too far. This is consistent with the idea, first presented in Levison & Morbidelli (2003), that Kuiper belt objects that we see were formed inside this boundary and that the full Kuiper belt — both cold and hot populations — was pushed outwards during the evolution of the planets. Since this idea so nicely solves the Kuiper belt’s mass depletion problem, our goal is to determine whether it is still viable in light of the Nice model. The issue is that Neptune’s evolution, as envisioned by this model, is substantially different from the smooth low-eccentricity migration contemplated in previous works.

The mechanism in Gomes (2003) for the push out of the hot populations might still work in the framework of the Nice model. Indeed, a massive scattered disk is produced and Neptune has a final phase of slow migration on circular orbit, which are the essential ingredients of Gomes’ mechanism. However, the mechanism proposed by Levison & Morbidelli (2003) for pushing out the cold population is in significant trouble. For this mechanism to work, Neptune’s 1:2 MMR must have been within the disk as Neptune began a phase of smooth outward migration. Since the outer edge of the disk is at ~ 34 AU, this implies that the semi-major axis of Neptune had to have been within ~ 21 AU at this time. The semi-major axis of Neptune after the last encounter with Uranus varies greatly from simulation to simulation of the Nice model (even if the final position of the planet is systematically at ~ 30 AU). However, in none of the successful simulations that we have produced did Neptune ever have a semi-major axis as small as 21 AU when it stopped having encounters with the other planets.

Therefore, we need to find another mechanism for the implantation of the cold

population in the Kuiper belt. This mechanism is detailed in the next section and makes use of the new aspect of Neptune’s evolution: a transient phase when its eccentricity was large.

3. A new transport mechanism to fill the Kuiper belt

In this section we describe a new mechanism for the outward transport of material from the primordial proto-planetary disk interior to 30 AU to the current Kuiper belt. This new mechanism is based on a well-known characteristic of the trans-Neptunian regions — Neptune’s MMRs are sticky (Holman & Wisdom 1993; Levison & Duncan 1997). In particular, integrations of test particles in the current scattered disk show that objects commonly become temporarily trapped in MMRs with Neptune, which can drive the particle’s eccentricity to low values, thereby decoupling them from Neptune (for example, see Levison & Duncan 1997, Fig. 7). In the current Solar System, these decoupling events can only occur at very specific and narrow ranges of semi-major axes because the mean motion resonances are narrow. In addition, since the orbits of the planets are not evolving, the process is time reversible and so there is no permanent capture.

However, the situation looks very different if Neptune’s orbit is eccentric because the region of semi-major over which objects can be decoupled from Neptune is much larger. This occurs for two reasons. First, Neptune’s large eccentricity forces extensive secular oscillations in the eccentricity of a particle in this region, thereby allowing it’s orbit to become temporally nearly circular at some locations. We find that for the values of eccentricity that we see in the Nice model simulations, these secular effects can be important in the 40 to 50 AU region. However, it takes longer than 2 Myr for the eccentricity to drop and thus this process is probably only important when Neptune’s damping time is long.

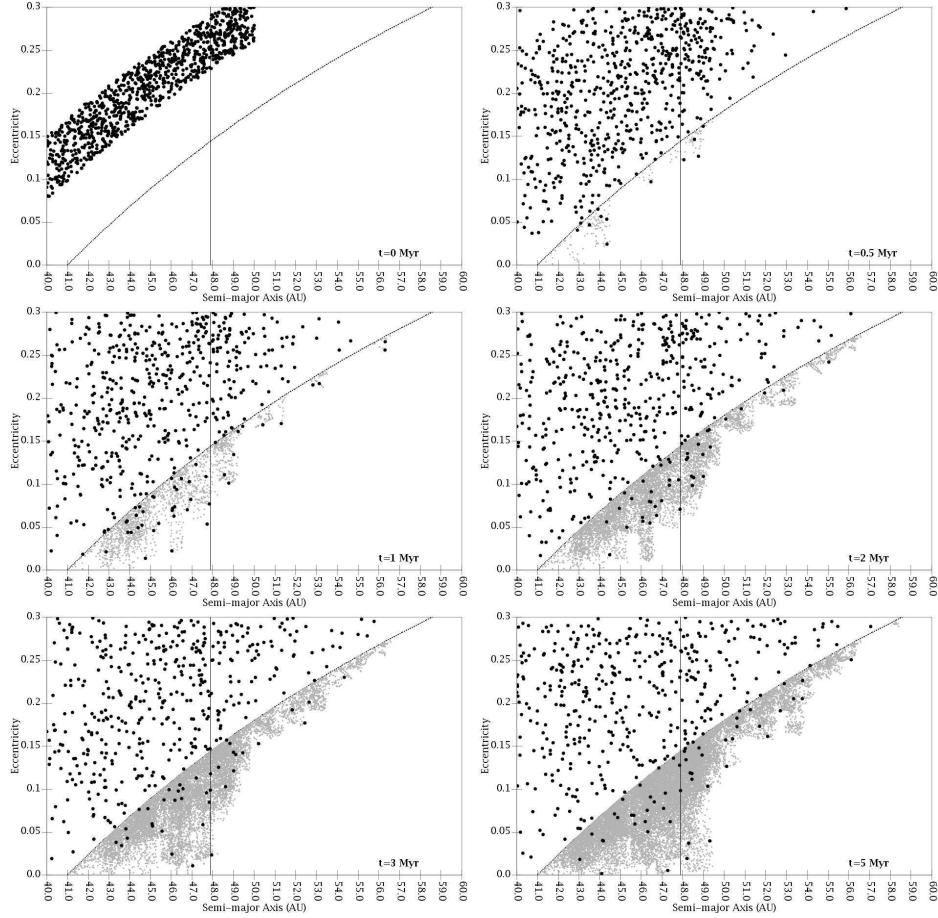


Fig. 3.— Evolution of particles undergoing perturbations from Neptune on an eccentric orbit ($a = 30$ AU, $e = 0.2$). The big dots represent the test particles, initially all on Neptune crossing orbits. The solid curve marks $q = 42$ AU and the dotted vertical line the location of the 1:2 MMR with Neptune. The area cumulatively visited by the particles in the $q > 42$ AU region is colored with small gray dots. Time evolves from the top left to the lower right panel. Because of overlapping resonances, particles can evolve into the Kuiper belt and acquire orbits with $e \sim 0$. In addition, the 1:2 MMR is a natural boundary of the visited region.

More importantly, when Neptune’s eccentricity is large the widths of all its mean motion resonances increase (see Morbidelli 2002). Indeed, numerical experiments of the

scattering process show that, for eccentricities larger than ~ 0.15 , the MMRs interior to the 1:2MMR overlap one another. Thus, there is literally a chaotic sea that extends outward from the orbit of Neptune to its 1:2 MMR through which particles can freely wander. For example, Fig. 3 shows the results of an experiment where Neptune is on an orbit with $a = 30$ AU and $e = 0.2$, and a number of test particles are initially placed on Neptune crossing orbits ($q < 36$ AU, see the top left panel of Fig. 3). As time passes, objects reach orbits with larger and larger q , and the region cumulatively visited by particles (painted with small gray dots in the figure) eventually covers the entire classical Kuiper belt. As expected, the 1:2 MMR provides boundary to this region (there are objects beyond the location of the center of the resonance because the resonance is very wide in this simulation). However, no particles are permanently trapped during this calculation because their trajectories are time reversible.

The dynamics illustrated in Fig. 3 allow us to envision a mechanism for the implantation of the cold population in the Kuiper belt in the framework of the Nice model. In fact, as described above, in the Nice model Neptune undergoes a transient phase during which its eccentricity is large. In many of our simulations of this model, this large eccentricity phase is achieved when Neptune has a semi-major axis of 27–29 AU, after its last encounter with Uranus. In these cases, a large portion of what is now the Kuiper belt is already interior to the location of the 1:2 MMR with Neptune. Thus, it is unstable, and can be invaded by objects coming from within the primordial disk (i.e. interior to ~ 34 AU). When the eccentricity of Neptune damps out, which takes between ~ 0.3 and ~ 4 Myr, the mechanism that causes this chaos disappears. The Kuiper belt becomes stable, and the objects that happen to occupy it at that time remain trapped for eternity.

Going back to the original simulations of the Nice model, we found several cases in which the above mechanism for the implantation of objects into the Kuiper belt was,

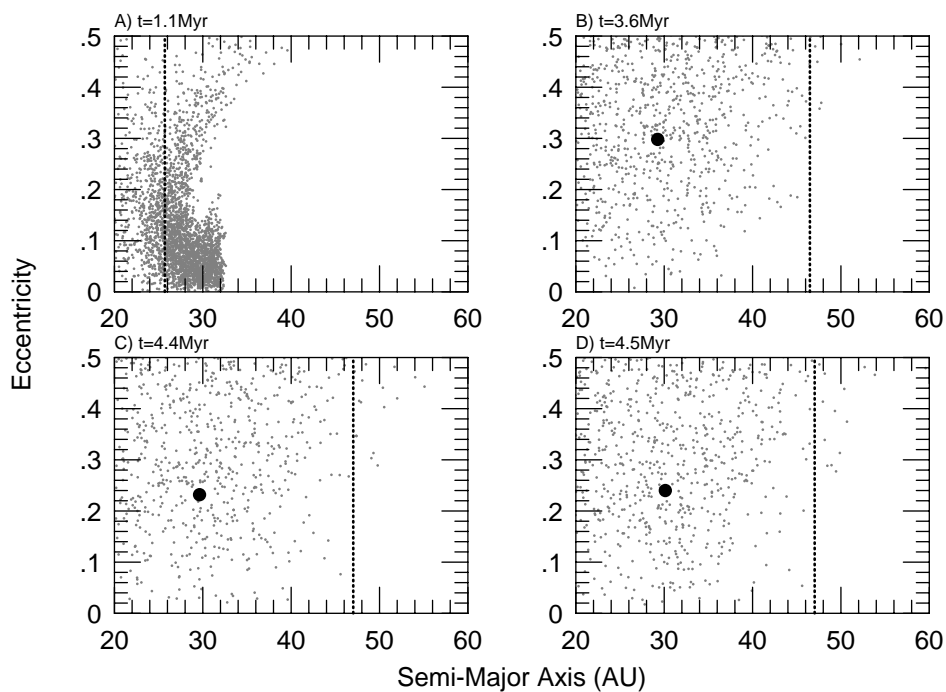


Fig. 4.— Snapshots taken from one of the simulations of the Nice model in Tsiganis et al. (2005). The big black dot represents Neptune, the small gray dots the particles and the vertical line the location of the 1:2 MMR with the planet at the corresponding time (reported in the upper left corner of each panel). For illustrative purposes in the last 3 snapshots we have rescaled the semi-major axis unit so that the final position of Neptune in this simulation is the current one. Time, t , is measured since the onset of the instability of Uranus and Neptune.

indeed, at work. Figure 4 gives one example. Figure 4A corresponds to the time when the planetary instability has just started. As one sees, the planetesimal’s disk is naturally divided in two parts: 1) the region inside the 1:2 MMR, which is excited as a result of the previous mean motion resonance sweeping and the onset of the planetary instability; and 2) the region beyond the 1:2 MMR, which remains relatively dynamically cold. Figure 4B shows the system just after the last encounter between Uranus and Neptune. Neptune has been kicked outward and onto a large eccentricity orbit. Consequently, the 1:2 MMR with Neptune is in the Kuiper belt. The main Kuiper belt region ($q > 36$ AU and $a < 48$ AU) is totally empty. Very rapidly, however, particles start to penetrate into the Kuiper belt due to the reasons described above (Figure 4C). When the invasion of particles is complete, the 1:2 MMR appears as a clear outer boundary of the low eccentricity population (Figure 4D).

Unfortunately, in all the simulations that we performed of the Nice model, the number of objects left in the classical Kuiper belt at the end of the simulations was too small to be analyzed. We believe that there are two reasons for this; both related to the fact that we used a relatively small number of disk particles. First, we do not expect the capture efficiency to be very large and thus we should not have captured many objects. Perhaps more importantly, the Neptune’s orbital evolution had a stochastic component that was too prominent, due to the fact that the disk was represented by unphysically massive objects. Therefore, in the next section we perform new simulations where these problems are rectified.

4. Simulated orbital distributions

As described above, self-consistent N–body simulations of the Nice model, such as those in Tsiganis et al. (2005), simply cannot be used to study the origin of the Kuiper belt. Thus, we decided to run *customized* simulations. In these simulations, the planets do not

gravitationally react to the small bodies, which are treated as test particles. The desired evolution of the planets’ semi-major axes, eccentricities and inclinations is obtained by the application of suitable fictitious forces added to their equations of motion. In particular, we employ the forces described in Malhotra (1995) for evolving semi-major axes and those in Kominami et al. (2005) for controlling eccentricity and inclination. In addition, since Uranus and Neptune are often started on crossing orbits and we want to avoid chaotic evolution due to close encounters, we soften the gravitational forces (\mathbf{f}_{UN}) between these two planets so that

$$\mathbf{f}_{UN} = \frac{Gm_N m_U}{(\mathbf{x}_{UN}^2 + \epsilon^2)^{3/2}} \mathbf{x}_{UN}, \quad (1)$$

where \mathbf{x}_{UN} is the relative position vector of Uranus and Neptune, m_N and m_U are their masses, and ϵ is a constant which we set to 0.8 AU. In this way, the evolution of the planetary orbits is smooth.

The above technique has another important advantage — we have precise control over the evolution of the planets. In the purely N-body simulations in Tsiganis et al. (2005), the evolution of the orbits of the planets is very chaotic. Changing the initial conditions by a very small amount can lead to a drastically different evolution of the system. Our techniques will allow us to change one aspect of the evolution from one run to the other, and study the effect of this one change on the resulting Kuiper belt. Moreover, if we realize that some simulations need more particles in order to get adequate statistics, we can run it again with additional test particles, and the evolution of the planets will not change.

In the following, we describe, in detail, the three main simulations that we performed, and comment also on two other test runs that we did for completeness. Each simulation originally contained 60,000 particles and was run for a billion years. In all, each took at total of 2 CPU years to complete. Thus, we could only perform a few runs and a complete exploration of parameter space is not feasible.

4.1. Run A

The initial conditions of all our runs are intended to mimic the state of the system immediately after the last encounter of Neptune with Uranus. In Run A, we assume that Neptune has $a = 27.5$ AU and $e = 0.3$, and Uranus has $a = 17.5$ AU and $e = 0.2$. The inclinations of both planets are small, of order 1 degree, consistent with many of the Nice model simulations after the last encounter between Uranus and Neptune (the conservation of the angular momentum tends to decrease the inclinations of the planets when they scatter each other onto distant orbits). Jupiter and Saturn were placed on low-eccentricity, low-inclination orbits with semi-major axes of 5.2 and 9.6 AU, respectively. The eccentricities of Uranus and Neptune are assumed to damp on a timescale of roughly 1 My, although the evolution of the planets are more complicated than this due, in part, to the interaction of the planets. The detailed evolution of the planets is shown in Fig. 5.

Before we continue, we must discuss one decision we made concerning the evolution of Uranus’ orbit that affects our resulting Kuiper belts. In the real Solar System, the ν_8 secular resonance is at 42 AU. This resonance is very strong and thus can remove objects on very short timescales (Duncan et al. 1995). Since the location of this resonance is very sensitive to the semi-major axis of Uranus, and Uranus is moving in our simulations, we were concerned that the ν_8 might inadvertently sweep through the classical Kuiper belt during our integrations thereby unintentionally contaminating the experiment. To avoid this, we forced Uranus to migrate a little too far from the Sun and arrive at its final location a little sooner than Neptune (see Fig. 5). Thus, in all our simulations Uranus final semi-major axis is slightly larger than observed and thus the ν_8 will be too close to the Sun.

The initial conditions for the disk were inspired by what we see in the simulations of the Nice model. As we have seen in Fig. 4A, the disk is naturally divided into an inner hot part and an outer cold part, with eccentricities up to 0.2–0.3 and 0.1–0.15, respectively.

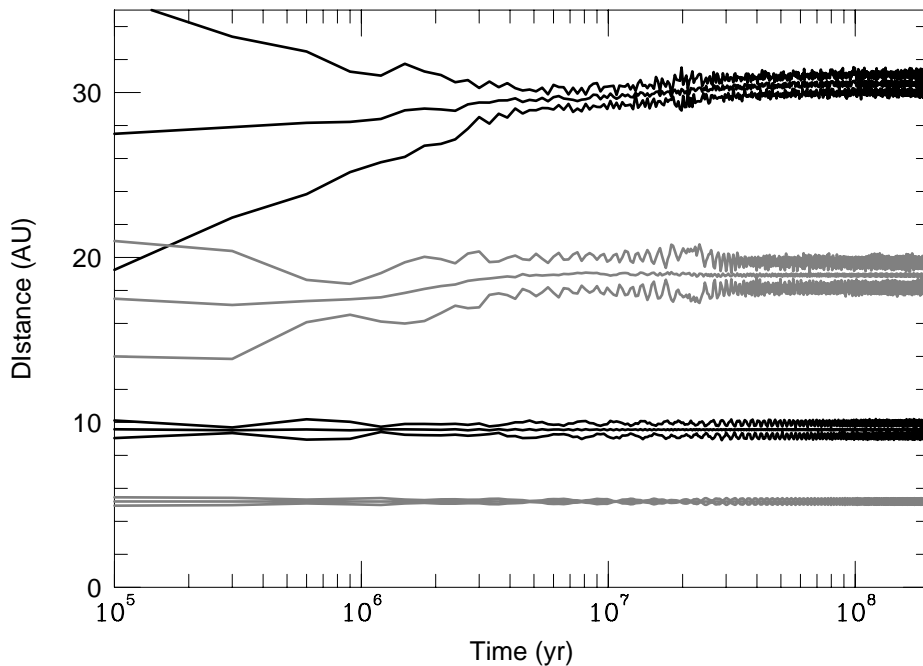


Fig. 5.— The imposed evolution of the giant planets in run A. Each planet is represented by three curves. The middle one corresponds to the value of the semi-major axis, the lower one to the value of the perihelion distance q , and the upper one to the value of the aphelion distance Q .

The boundary between these two disks is at the location of the 1:2 MMR with Neptune at the time of the planetary instability, typically at $a \sim 29$ AU. The inclinations are also more excited in the inner part than in the outer part. At the time when Uranus and Neptune become unstable, the outer part essentially preserves the initial inclinations of the disk (0.5

degrees in the simulations of the Nice model).

The initial orbital distribution of our disk particles is an idealized version of what we see in Fig. 4A. In particular, we placed particles on orbits with semi-major axes between 20 and 34 AU. In the inner disk, which we take to be inside of 29 AU, the eccentricity of the particles is assumed to be equal to 0.2, and the inclination to have a differential distribution of the form

$$\sin(i) e^{-i^2/2\sigma_i^2}, \quad (2)$$

with $\sigma_i = 6^\circ$. Our specific choice of the inclination distribution in the inner disk is inspired by the results of the Nice model simulations (Tsiganis et al. 2005, see Fig. 4A), but as we discuss in more detail below, this value is not crucial. In the outer disk, the eccentricity of the particles is assumed to be equal to 0.15 and the inclination is assumed to be 0. An equal number of particles (30,000) is used to model both the inner and the outer disk.

Our calculations were performed in two steps. During the first time-span of 200 My, the simulations were done using a variant of `swift_rmvs3` (Levison & Duncan 1994) that incorporates the fictitious forces described above. Thus, the planets migrate and circularize in these calculations. We then continued the simulation to a billion years without any migration or damping imposed on the planets, in order to eliminate scattered disk particles and the bodies that were marginally unstable in the Kuiper belt. For this second simulation we used the code `swift_whm`, which executes the algorithm presented in Wisdom & Holman (1991). During the second phase, Particles were removed from the simulation when they encountered a planet within a distance of one Hill radius.

Fig. 6 shows the $a-e$ and $a-i$ distributions of the particles surviving at the end of one billion years. The color of a particle indicates its dynamical class. This is determined by following the procedures outlined in Gladman et al. (2007), where each object is classified by a process of elimination using an integration of a 10 Myr. First, we checked if an object

is ‘Scattering,’ by which we mean that its barycentric semi-major axis varies by more than 1.5 AU over the length of the integration. Next we look for resonance occupation. Determining if an object is in a mean motion resonance with Neptune is not a trivial task. An object is classified using the resonant argument, ϕ_{mn} , for each $n:m$ MMR. Resonances with $n \leq m < 30$ are considered. In addition, a given resonance is checked only if the object in question is within 0.5 AU of its location. We split the 10 Myr integration in to 20 equal sections. If ϕ librates in all of these, by which we mean it never has ϕ_{mn} more than 179.5° away from the libration point, the object is classified as ‘Resonant’. If an object’s ϕ_{mn} librates in at least 15 of the 20 sections then it is flagged as possibly resonant and needing to be double checked by eye. The failure to librate in a given section is often because the eccentricity of the object drops and ϕ_{mn} becomes ill defined. Fortunately, this only occurs to a small fraction of our objects. In the figure, the dots that are black represent objects in one of Neptune’s mean motion resonances, dots that are green are ‘Scattering’ objects, and the red dots are non-resonant stable objects.

We start our discussion with the $a-e$ distribution, which is shown in Fig. 6A. This distribution looks similar to the one we observe (compare with Fig. 1A). In particular, three main features are reproduced: (i) the edge of the classical belt at the 1:2 MMR, (ii) the deficiency of nearly-circular objects in the region immediately interior to the 1:2 MMR, (iii) the extended scattered disk. Also, all the main MMR with Neptune are populated, including those beyond the 1:2. To our knowledge, this is the first simulation that reproduces the observed $a-e$ distribution of the trans-Neptunian population so nicely.

Nevertheless, a more accurate comparison between simulation and observations shows a couple discrepancies:

- the 40–42 AU region is not depleted, particularly at low inclination. The depletion of the real distribution in this region is due to the presence of the secular resonances ν_8

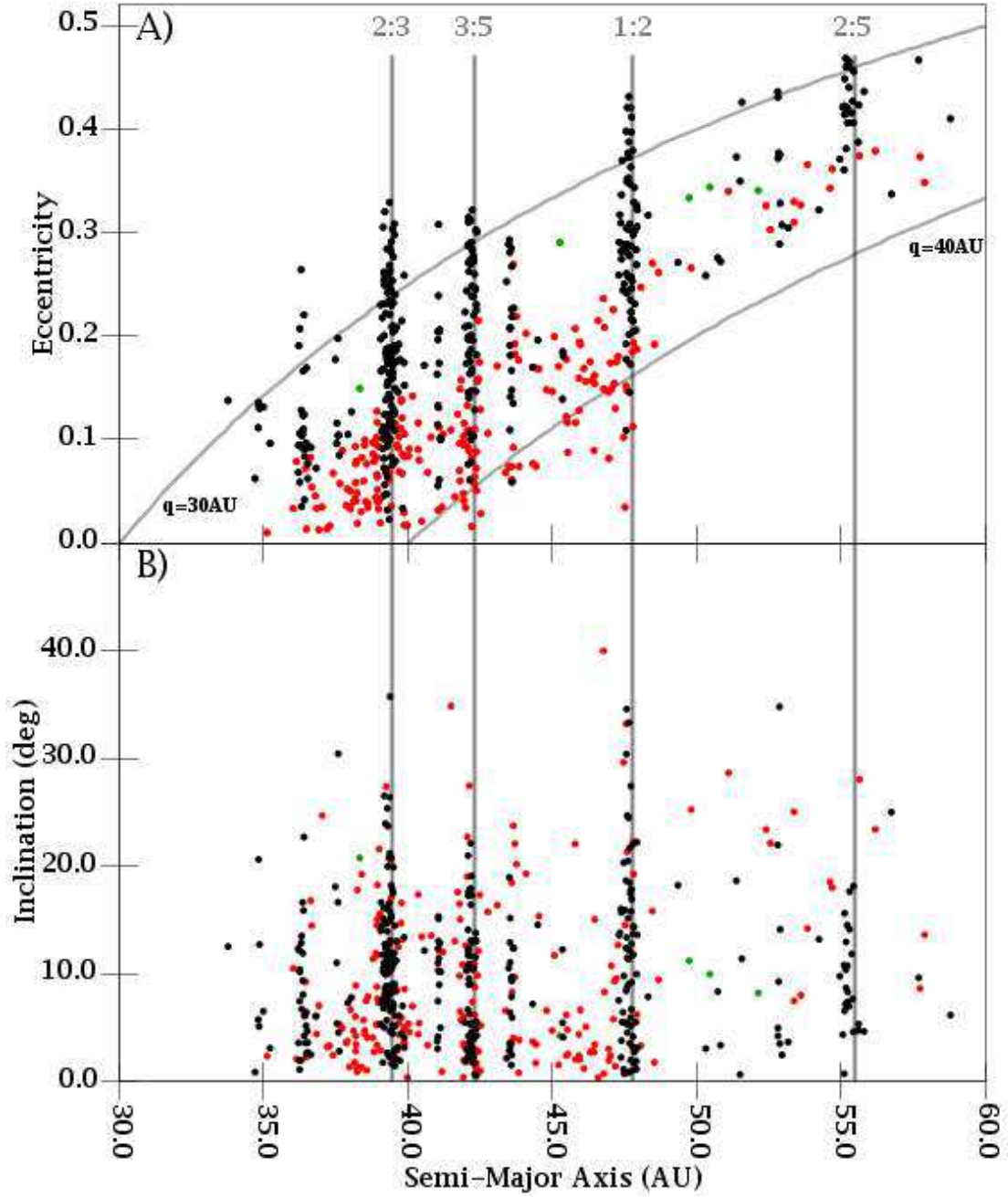


Fig. 6.— The semi-major axis versus eccentricity (A) and semi-major axis versus inclinations (B) distributions of the particles captured in the trans-Neptunian region in Run A. See Fig. 1 for a description.

and ν_{18} (Duncan et al. 1995; Morbidelli et al. 1995). As described above, by design these resonances are not present at the same location in our model because the orbits of the planets, particularly Uranus, are not located exactly at the correct places.

- the classical belt (red dots in the figures) appears to be somewhat too excited in eccentricity. In particular, although the basic shape of the a - e distribution follows the observations — nearly-circular objects out to some semi-major axis and then e increasing with a — the location where the nearly-circular orbits stop (which we call a_C) is too close to the Sun. In particular, real low-eccentricity KBOs can be seen to roughly 45 AU (Fig. 1), while in Run A this population stops at 43 AU.

The last problem is probably the most serious. In order to perform a quantitative comparison between the model and the observed eccentricity distributions in the classical belt, we have implemented a bias calculator algorithm inspired by the work of Trujillo & Brown (2001). This method takes as input: 1) orbital element distribution from a model, 2) an assumed absolute magnitude distribution, and 3) the observed magnitudes and latitudes of the population being modeled. From this, it predicts what the observed orbital element distribution of the population should be according to the model. It is described in some detail in Morbidelli & Brown (2004), Morbidelli et al. (2004) and Fernandez & Morbidelli (2006). We apply it to the population of non-resonant objects with $42 < a < 48$ AU in order to avoid the issue, discussed above, of where we placed the ν_8 secular resonance. For the real Kuiper belt objects, we only include objects that have been observed over multiple oppositions in order to guarantee that the orbits are well determined. In the calculation, we assume that each particle represents full population of objects, with cumulative absolute magnitude distribution

$$N(<H) = C10^{0.6H} , \tag{3}$$

(Gladman et al. 2001), where C is an arbitrary constant (the same for all particles). We

find that if our model were correct, the median eccentricity of the observed classical belt bodies would be 0.11, whereas the median eccentricity of the real objects is 0.07. Although not large, this discrepancy is statistically significant.

We can get some insight into how we might fix the above problem by discussing the origin of a - e distribution in our models. Recall that this distribution is characterized by low-eccentricity objects out to a_C and beyond this distance e increases with a . However, $a_C = 43$ AU in Run A, which is too small.

Also recall that in this simulation, Neptune starts with $a = 27.5$ AU and $e = 0.3$. It slowly migrates outward and its eccentricity decreases with time. The fact that the eccentricity damps implies that the region interior to Neptune’s 1:2 MMR is most chaotic at the beginning of the simulation when the resonance is at 43.6 AU. Thus, the region inside of this distance is filled with objects. As the system evolves, the resonance moves outward. At the same time, however, Neptune’s eccentricity decreases, and so, the region immediately interior to the 1:2 MMR becomes more stable. As a result, we expect fewer low-eccentricity objects beyond 43.6 AU because as the resonance migrates through this region, the chaotic region shrinks. This argument predicts that $a_C \sim 43.6$ AU, which is roughly what we see. If it is correct, we can move a_C outward by starting Neptune further from the Sun. We present such a simulation in sect. 4.2, below.

The magnitude of the Plutino population is an other important constraint on the models. Unfortunately, here the observations are not clear. Trujillo et al. (2001) estimate that only roughly 10% of the total population of the Kuiper belt are in all the resonances combined. On the other extreme, Kavelaars et al. (2007) put the fraction of objects in Neptune’s 2:3 MMR alone at $\sim 20\%$. For this model, we find that 21% of the particles within $a = 50$ AU are in Neptune’s 2:3 MMR. Thus, if Kavelaars et al. is correct, our model is fine. We address this issue again in sect. 6.2.

As discussed above, the inclination distribution of the classical belt is also an important diagnostic. To compare the distribution obtained by our model with the observations, we again use the Trujillo-Brown-like bias calculator mentioned above. As before, we select real objects and simulation particles that are non-resonant and have $42 < a < 48$ AU. In addition, in order to remove the effects of changes in size distribution with inclination, we only considered objects with absolute magnitudes, H , fainter than 6 (we took a slightly fainter magnitude than Levison & Stern 2001’s nominal value in order to be conservative). The result of this calculation is presented in Fig. 7A.

The black curve in Fig. 7A shows the cumulative inclination distribution of the observed objects. The gray curve represents the cumulative inclination distribution expected from our model once the biases are taken into account using the bias calculator described above. As one sees, the agreement is quite good, particularly up to 10 degrees. This means that we have correctly reproduced the existence of a cold population — in particular the inclination distribution within the cold belt. We also produce the correct number of high-inclination objects. Indeed, the highest inclination object in our model is 34° , which can be compared to 31° in the observed dataset. A Kolmogorov-Smirnov (KS) statistical test (Press et al. 1992) between the two curves in Fig. 7A says that they have a 57% chance of being derived from the same distribution¹, which is excellent.

¹To be more precise, a KS probability of 0.57 means the following. Assume that there was a single parent distribution for both the model and the observations. In particular, the model was a random sample containing, say, J entries, while the observations contained K entries. If we were to generate two random representations of this parent population, one with J entries and one with K , there would be a 57% chance that the comparison between these random populations would be *worse* than what we observe in Fig. 7A. This, despite the fact that these new distributions were directly derived from the parent. Therefore, the agreement between our model and the observations is very good. Indeed, any comparison

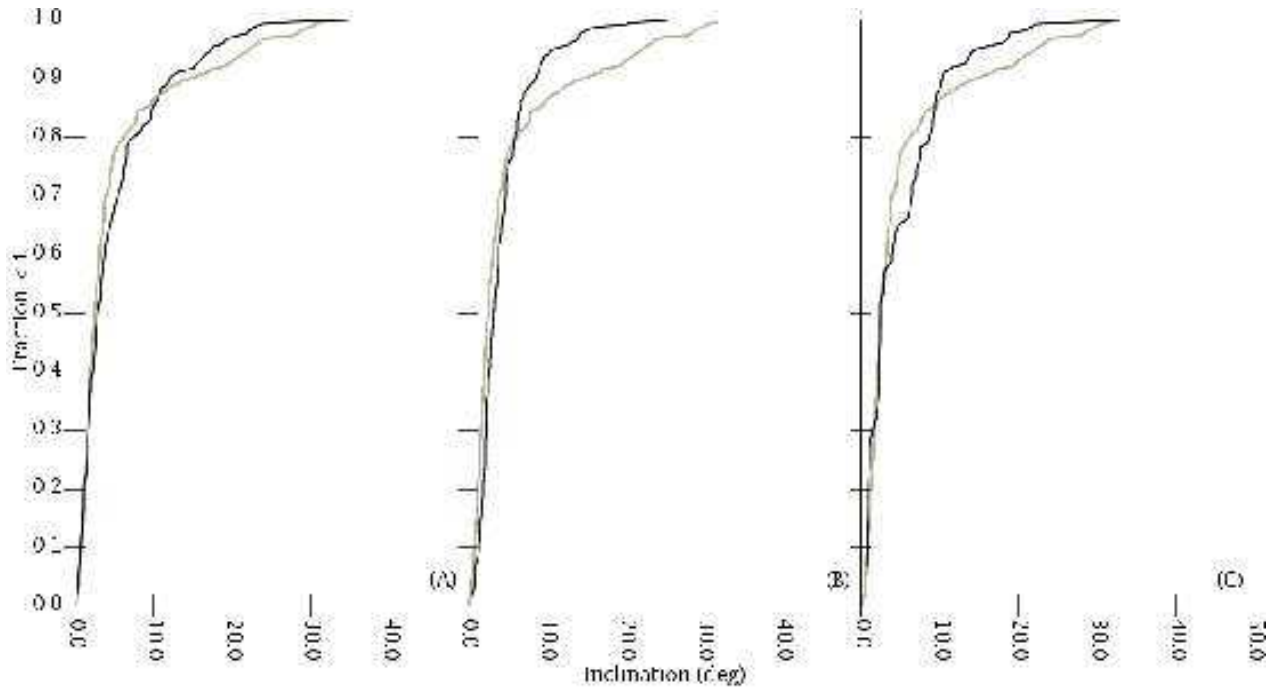


Fig. 7.— The observed cumulative inclination distribution of the observed classical belt objects (solid curve) and that expected from the result of our simulation (gray curve). Both datasets include observational biases. A) run A. B) run B. C) run C.

Insight into how the low-inclination objects are preserved can be gleaned by plotting the time at which an object is first captured into the classical Kuiper belt as a function of its final inclination. In particular, Fig. 8 shows that the implantation of particles in the Kuiper belt happens in two stages. The first stage occurs very rapidly, within the first ~ 2 My. The particles that are trapped in the Kuiper belt during this stage do so under the mechanism described in the previous section. As Fig. 8 shows, most of the particles captured at this early time have a low inclination. This is due to the fact that they have fewer encounters with Neptune. Indeed, we find a direct correlation between the number of

with a KS probability greater than ~ 0.1 should be considered acceptable, and values as small as ~ 0.05 (2σ) cannot be ruled out.

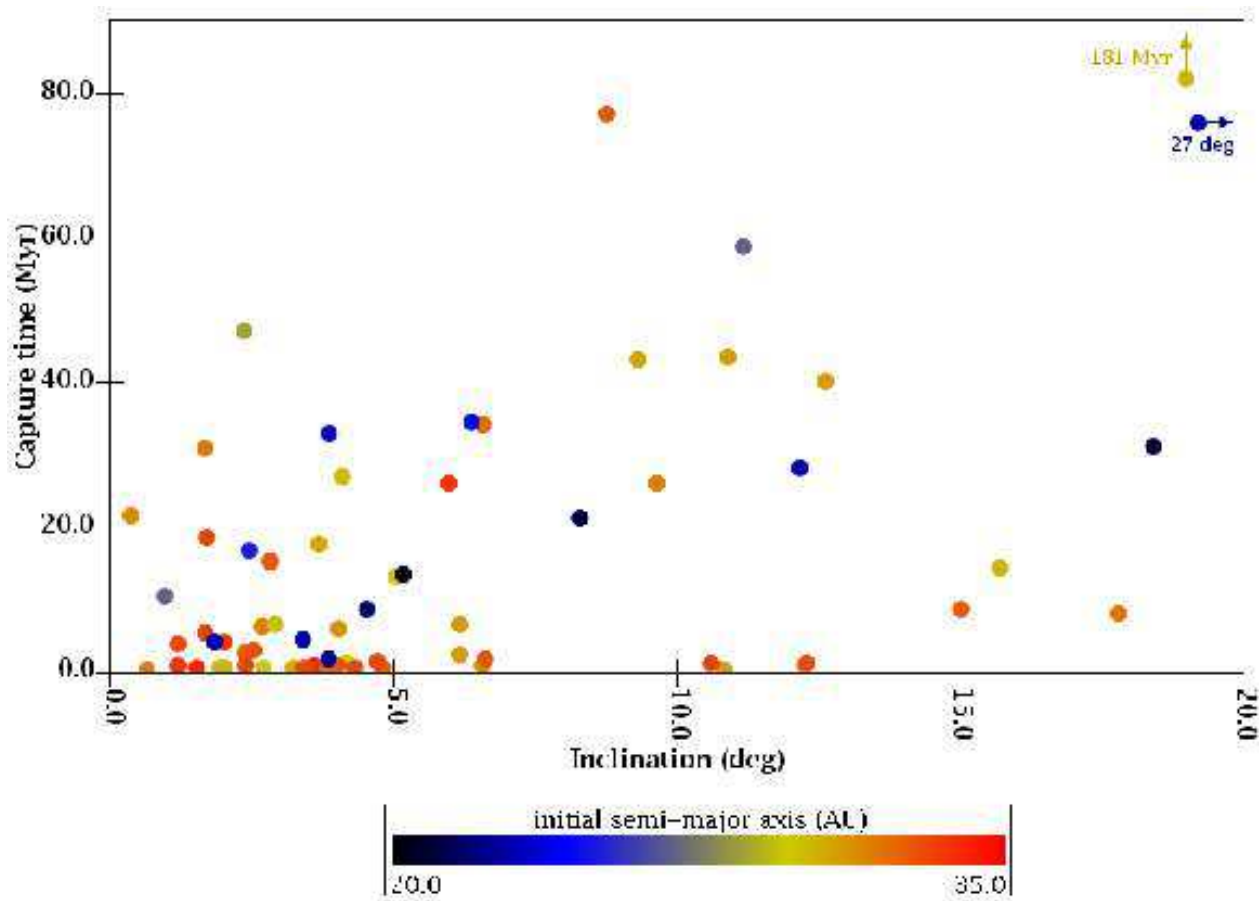


Fig. 8.— For the particles permanently trapped in the classical belt, this diagram shows the time of capture as a function of the final inclination. The color codes the original semi-major axis of the bodies.

encounters a particle has with Neptune and its final inclination in the Kuiper belt. There is a well defined cluster with $i < 5^\circ$ in Fig. 8, although some particles have inclinations up to 13° .

After a few million years the eccentricity of Neptune is damped enough that the resonances no longer overlap and the bulk of the Kuiper belt becomes stable. Thus, the capture mechanism described above can no longer function. The second stage of the capture process starts at this time, where particles are trapped via the evolutionary pathway

discovered in Gomes (2003). As Fig. 8 shows, the capture times of the particles during this second stage are more uniformly distributed, from a few million years up to 200 My. The inclination distribution of the bodies captured during the second stage does not show any preference for low inclination.

Fig. 8 also shows that, while the particles captured during the first stage come almost exclusively from the outer part of the disk, those captured during the second stage are mainly from the inner disk. We will come back to this in sect. 5.

4.2. Run B

This next run is designed to improve the a - e distribution of the classical belt objects over what was obtained in run A. In particular, we aim to extend the distribution of the circular objects trapped in the classical belt up to $a_C \sim 44$ AU in order to obtain a better agreement with the observations. The only major difference between this run and run A was that we placed Neptune initially at 28.9 AU instead of 27.5 AU. We did this so that the initial location of the 1:2MMR would be slightly beyond 45 AU, with the expectations that the first stage of the capture process — which fills the full a - e plane up to the resonance’s location — would implant objects onto nearly-circular orbits up to approximately 44–45 AU. We also adjusted the migration rate of Neptune so that its final semi-major axis is at 30.1 AU.

The results of this run are shown in Fig. 9. Indeed, our goal seems to have been achieved. The a - e distribution is more similar to the observations than that in run A (compare with Fig. 1A). The population of nearly-circular objects at low-inclination now extends to ~ 45 AU. The deficit of low-eccentricity objects between 45 and 48 AU is preserved, and the outer edge of the classical belt is still at the final location of the

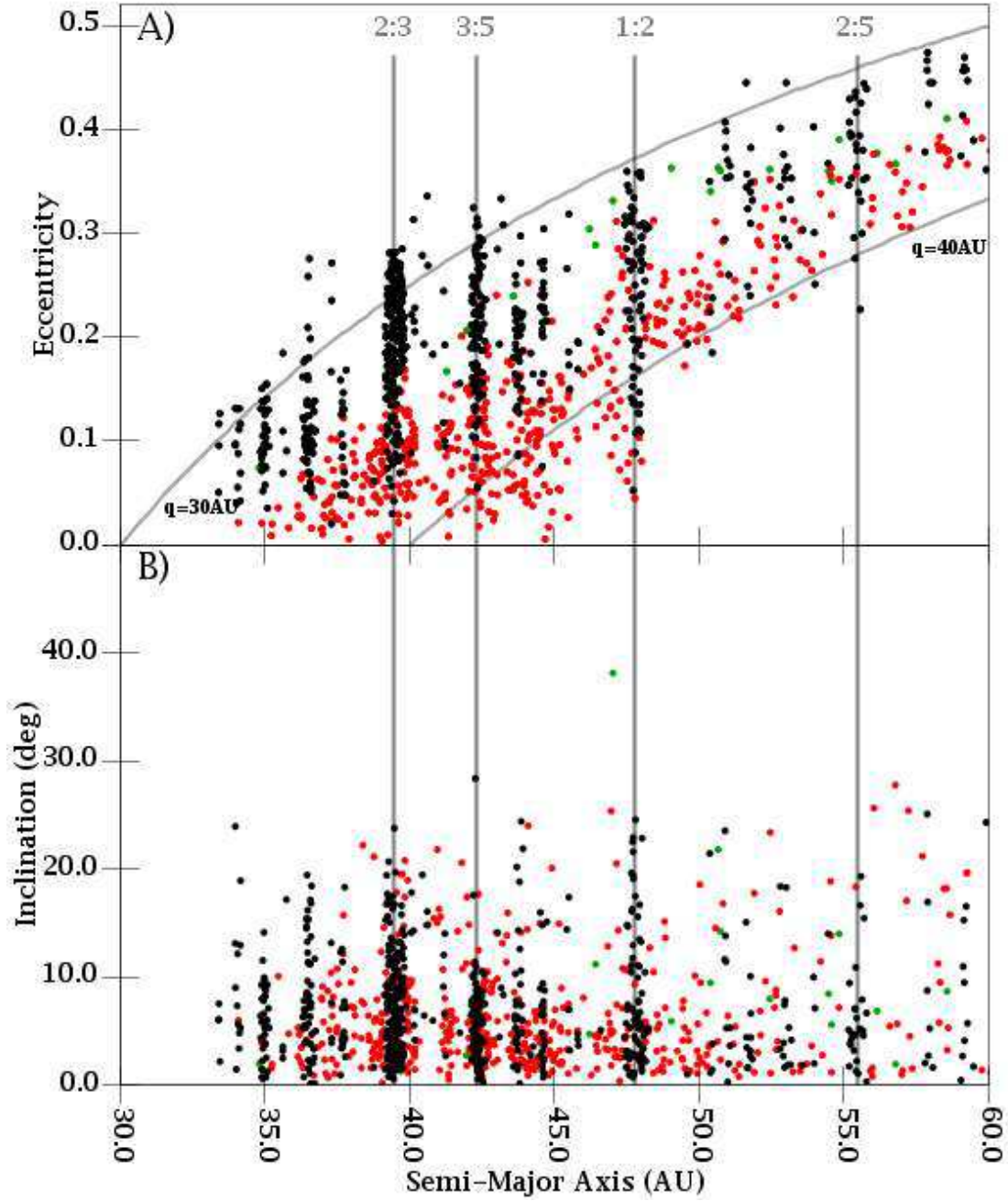


Fig. 9.— Same as Fig. 6, but for Run B.

1:2 MMR with Neptune. Moreover, beyond the 1:2 resonance, the extended scattered disk contains objects with larger perihelion distances than it does in run A, which is also in

better agreement with the observed distribution.

Nevertheless, when we run the simulated distribution of the classical belt through the bias calculator, and compare the resulting cumulative eccentricity distribution with the observed one, the match is still not perfect: This model predicts that the observed median eccentricity of the classical population should be 0.10, lower than what run A predicts (0.11), but still larger than the observed value of 0.07. Again, this difference is statistically significant.

Fig. 7B shows a comparison between the observed inclination distribution in the classical belt and the prediction of Run B after processing through the bias calculator. This case is not as good as that of run A. The deficit of large inclination bodies appears more prominent. The observed and the model distributions now diverge at $i \sim 6^\circ$, and the largest inclination among the captured bodies is only 25° . This is probably the consequence of the fact that we started Neptune at a larger semi-major axis, and thus it migrates a shorter distance. This, in turn, partially inhibits Gomes’s mechanism for capturing the hot population. The KS-test between the observed and the model distributions tells us that they only have a 4% chance of being two statistical representations of the same underlying parent distribution. Thus, this model can be ruled out at the 2σ level based on its inclination distribution. Nevertheless, the distribution of the inclinations in the cold population is in excellent agreement with the observations.

At this point, the natural question to ask is whether the poor inclination distribution of this model is the result of our initial conditions. Recall that we set $\sigma_i = 6^\circ$ (see Eq. 2) for the inner disk based on the N -body simulations in Tsiganis et al. (2005). This value is much smaller than the hot classical belt, which has $\sigma_i \sim 12^\circ$ (Brown 2001). Thus, we performed a simulation where we set the initial σ_i of the inner disk to 12° in order to see if we produced a more reasonable inclination distribution. Surprisingly, the classical

belt inclination distribution of this new run is very similar to the old. Thus, the poor performance of this model cannot be blamed on our initial conditions.

4.3. Run C

Another potential way of improving the a - e distribution over what we see in run A, is to increase the damping timescale of Neptune’s eccentricity. This might help because if Neptune’s eccentricity decays more slowly, the planet, and its 1:2 MMR, have the time to migrate further out before that the first stage of the trapping process (the one governed by the planet’s eccentricity) ends. Therefore, in this subsection we present the results of a simulation, run C, in which Neptune has the same initial semi-major axis and eccentricity as in run A, but the eccentricity damping timescale that is roughly 3 times longer.

The resulting a - e distribution is shown in Fig. 10. Like, run B, this distribution matches the observations better than does run A in that we have objects with $e \sim 0$ out to 45 AU. The median eccentricity of the classical objects, according to this model after accounting for observational biases, should be ~ 0.13 , which makes it the worst of the three models.

On the other hand, the inclination distribution appears to be reasonable. As Fig. 7C shows, the model distribution appears hotter than the observed distribution between 3 and 10 degrees. This means that there are too many objects at moderate inclinations (4 to 10 degrees) compared to high inclinations (greater than 20 degrees). However, this model does contain objects with inclinations as large as 33° and the KS-test between the two curves in Fig. 7C concludes that the probability that the two distributions are statistically equivalent is nevertheless 0.35%.

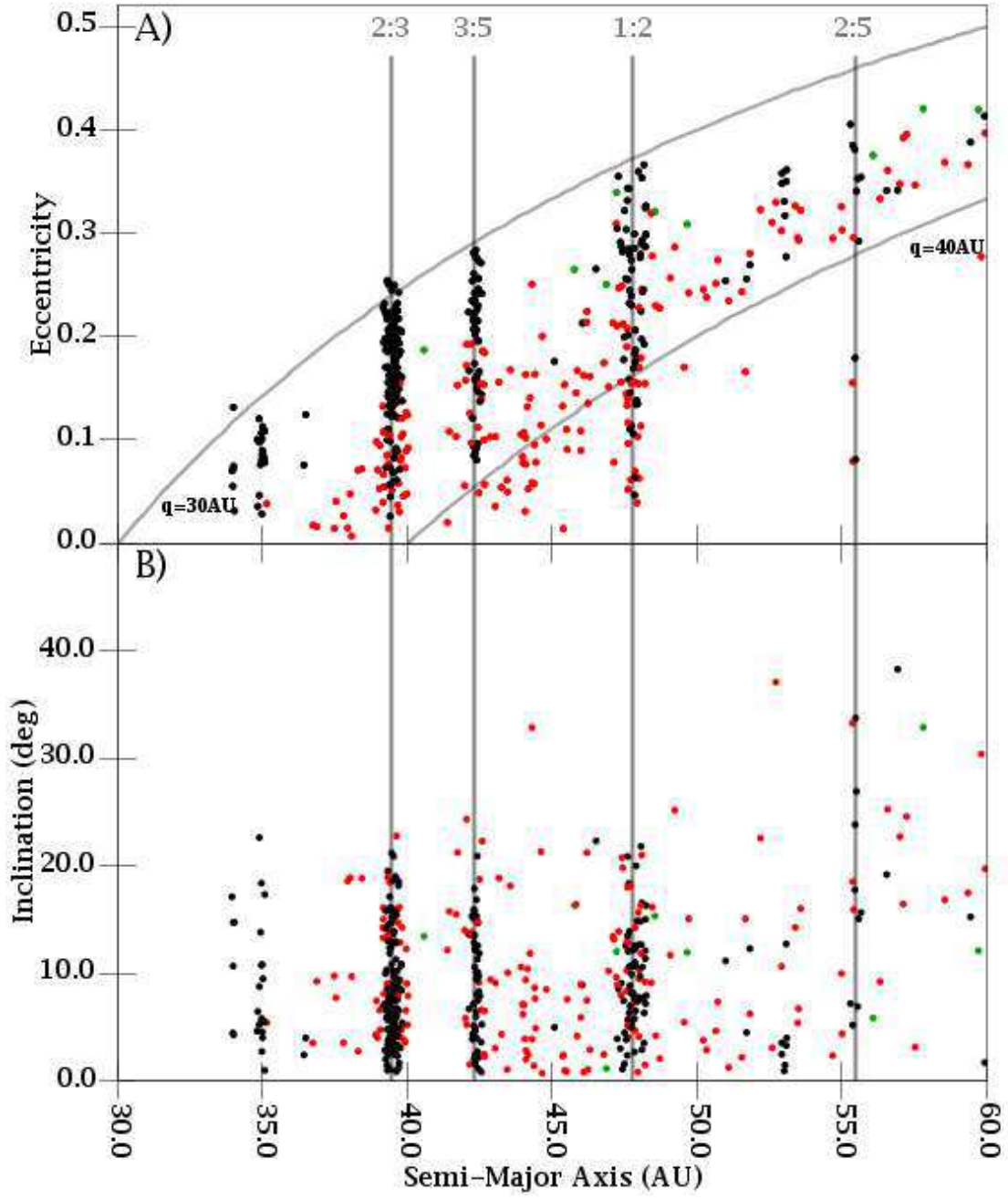


Fig. 10.— Same as Fig. 6, but for Run C.

4.4. Other runs

In addition to the three runs described above, we have performed two additional runs in order to better explore the parameter space and the effects of these parameters on the resulting Kuiper belt structure. These runs are not discussed in much detail because they were less successful than the runs described above.

In run D, we used the same configuration as in run A, but we *decreased* the eccentricity damping timescale by about $1/3$ to $\sim 400,000$ yrs. In other words, run D stands on the opposite side of run A than does run C with regard to the damping time. Run D did not create a classical Kuiper belt at all. This result is not surprising, because as Fig. 3 shows, it takes roughly a million years for the particles to penetrate the Kuiper belt, and thus, Neptune’s eccentricity damps too fast in this run so that the particles do not have enough time to penetrate into the Kuiper belt before that the latter becomes stable.

Run E was set up to enhance the effect of Gomes (2003) mechanism. In particular, we set Neptune’s initial semi-major axis to 28 AU. In addition, Neptune’s eccentricity damping rate was set to 3 Myrs (like run C). However, Neptune’s migration was done in two stages. For the first 5 Myr, Neptune migrated as it did in run B, so that at the end of this stage it was at 29.2 AU. Then, Neptune migrated very slowly, reaching 30.1 AU in about 100 Myr. In this run we found that the population of nearly circular classical bodies extends to larger semi-major axes, almost up to the 1:2 MMR location. The extended scattered disk beyond the 1:2 MMR extends to larger perihelion distance, so that there is almost no apparent ‘edge’ at the 1:2 MMR in the resulting a - e distribution. Furthermore, the inclination distribution is too excited, so that the cold population is under-represented. Nevertheless, the number of bodies captured at high inclination is not significantly higher than it was in run B. Thus, the goal of this simulation was not achieved.

5. Origin of the correlations between physical and dynamical properties

As we reviewed in the introduction, the Kuiper belt displays two strong correlations between an object’s physical properties and its orbit. The first one is a relationship between absolute magnitude (or size) and inclination. In particular, the existence of a cold ‘core’ in the inclination distribution is visible only for those bodies with $H \gtrsim 6$ (Levison & Stern, 2001). Most bodies with $H > 6$ have $i < 4^\circ$. The second correlation is between colors and inclination. The cold population is deficient of objects with a neutral spectral gradient, often called ‘gray objects’ (Tegler & Romanishin 2000; Trujillo & Brown 2002; Doressoundiram et al. 2005). Because colors can be affected by evolutionary processes such as irradiation, heating, out-gassing, collisional resurfacing, we think that the correlation between size and inclination has better chances to be directly related to the origin and primordial sculpting of the Kuiper belt. Therefore, we first discuss the H versus i correlation.

Fig. 11 shows the final inclination of the particles trapped in the classical belt as a function of their initial semi-major axis (a_0), for our three main runs. In both Runs B and C, the low inclination ‘core’ (namely an over-density of objects with $i < 4^\circ$) is made of particles with $a_0 > 29$ AU. In our most extreme case (Run B), only 5% of the particles with $i < 4^\circ$ initially come from the region interior to 29 AU (we call this fraction f_{cold}), while most of the objects with $i > 15^\circ$ come from this region ($f_{\text{hot}} = 0.54$). For Run A these fractions are $f_{\text{cold}} = 0.07$ and $f_{\text{hot}} = 0.17$, and they are $f_{\text{cold}} = 0.11$ and $f_{\text{hot}} = 0.40$ for Run C. So, although there is large variation from run to run, there is always a trend that the low inclination particles formed further from the Sun than the high inclination ones.

Before we discuss the implications of the above result, we would like to understand its origin. It is partially a consequence of our initial conditions, which are based on the N-body simulations of the Nice model, where the outer disk is initially cold (low eccentricities and inclinations), whereas the inner disk is already excited. However, this cannot be the sole

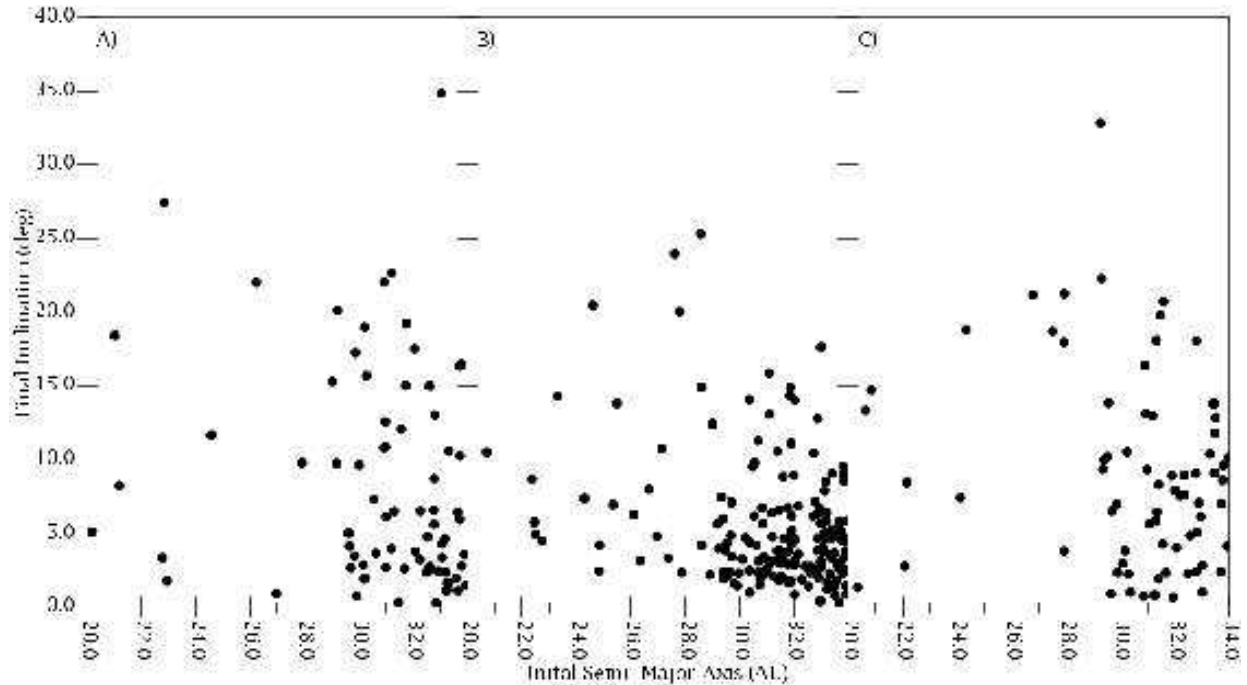


Fig. 11.— The final inclination as a function of the initial semi-major axis, for particles trapped in the classical Kuiper belt. A) from run A. B) from run B. C) from Run C.

explanation. If it were, we would expect that captured large-inclination Kuiper belt objects would have started the simulation with large inclinations in the inner disk. This is not seen. Therefore, the deficiency of low inclination particles from the inner disk cannot be simply explained by our initial inclination distribution.

Another important effect is that objects from the inner disk encounter Neptune more often than those from the outer disk. For example in run B, the captured classical Kuiper belt objects that originated in the inner disk encountered Neptune an average of 59 times, while those from the outer disk only encounter Neptune 19 times on average. Therefore, the orbital excitation due to the close encounters with Neptune is much more pronounced for objects from the inner disk, and so the chances to preserve an initial low inclination are smaller.

What ever its exact origin, the above result can explain the correlation between H versus i . It is natural to expect that the size distribution of the disk planetesimals was a function of heliocentric distance. In particular, given that the timescale for the growth of a body increases with increasing orbital period (Safronov 1969), it is legitimate to expect that some bodies in the inner part of the disk could acquire larger sizes than the largest of the bodies in the outer part of the disk. Let us assume, for example, that bodies with $H < 6$ could form only on orbits with, say, $a < 28$ AU. Fig. 11 shows that, for these bodies, the inclination distribution would be rather extended, with no low inclination ‘core’ — at least for Runs B and C. Therefore, our simulations explain, at least qualitatively, the H versus i correlation.

From a more quantitative point of view, the black curve in Fig. 12 shows the inclination distribution of all multi-opposition Kuiper belt objects with $H < 5.5$ (to be conservative, we took a slightly brighter magnitude than Levison & Stern’s limit). In order to get better statistics, here we included all objects with $32 < a < 50$ AU and $q > 31$ AU. For comparison, the gray curves plot what we would expect from our three main runs assuming that $H < 5.5$ objects only formed interior to 27 AU. The KS probabilities are 0.42, 0.24, and 0.17 for runs A, B, and C, respectively, and thus the agreement is very good. Thus, our model supports the idea that big objects, or at least intrinsically bright ones, originated closer to the Sun.

We now come to the issue of the colors. Let us assume, for simplicity, that there are no evolutionary processes, and, for some unknown reason, the objects that formed in the inner parts of the disk are gray and those from the outer parts are red. As we discussed above, our simulations produce a classical Kuiper belt where a higher fraction of objects with $i < 4^\circ$ come from outer disk than the high inclination objects. This fact is most pronounced in run B, where $f_{\text{cold}} = 0.05$ and $f_{\text{hot}} = 0.54$. Thus, this model predicts that 95% of the cold population would be red, while the hot population would be roughly 50-50.

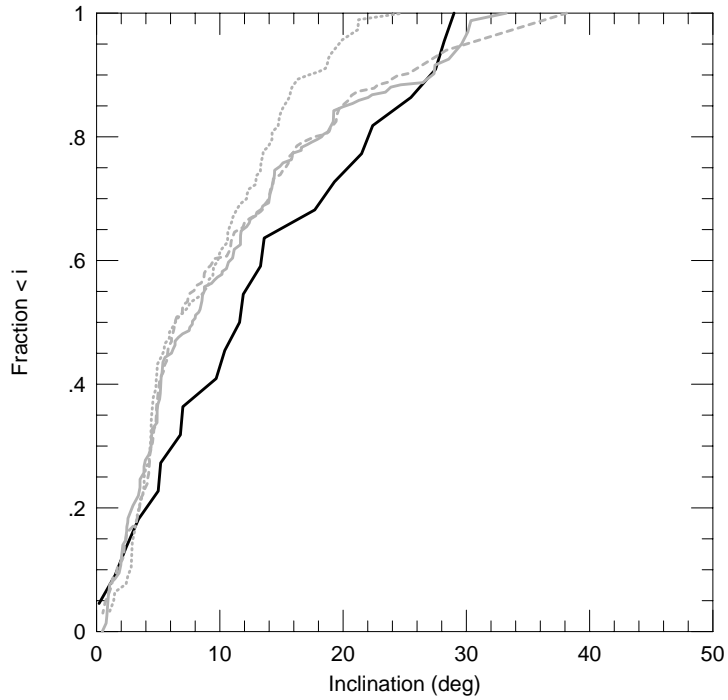


Fig. 12.— The cumulative observed inclination distribution for the bright objects in the Kuiper belt. The black curve shows all multi-opposition objects with $32 < a < 50$ AU, $q > 31$ AU, and $H < 5.5$. The dashed, solid, and dotted gray curves show fictitious objects from Runs A, B, and C, respectively, which were trapped in the same region of space. For the models, however, we only included those objects with initial $a < 27$ AU. In addition, we ran the models through our survey simulator.

Nevertheless, even run B would predict that we should be finding some gray objects among the cold population, and our other runs would argue for significantly more. Observations, conversely, seem to show a total absence of gray objects in the cold ‘core’. Having said this, we believe that the total lack of gray low-inclination objects is either a statistical fluke, or, more likely, an indication that the colors are not primordial. This is due to the fact that, independent of the Nice model, it is difficult to imagine a dynamical mechanism that can create a population of objects *only* at high inclination. Any mechanism that we can think of will naturally include some low-inclination objects and therefore there should be some gray bodies in the cold population if color is primordial.

As described above, there is also a correlation between color and perihelion distance in that all objects with $q > 39$ AU are red (Doressoundiram et al. 2005). The bodies coming from the inner disk tend to acquire final perihelion distances that are smaller than the objects from the outer disk. Therefore, if we look at bodies with $q > 39$ AU, the ratio of outer disk to inner disk bodies should be smaller than, say, for $36 < q < 39$. In fact, we find that in run B all the bodies trapped in the Kuiper belt with $q > 40$ AU come from the outer disk. Thus, if colors are primordial and are a function of formation heliocentric distance, our models can explain these observations.

In conclusion, the results are somewhat mixed when it comes to whether our models can produce the relationship between orbit and physical characteristics. As Fig. 12 shows, in all three models the inclination distribution of objects that formed interior to 27 AU is consistent with the observed distribution of intrinsically bright KBOs. However, only run B, and perhaps run C, can convincingly explain the correlation between colors and inclination. As we discussed above, we believe it likely that some evolutionary processes, yet to be understood, created, or at the very least, sharpened the correlations between color and orbit. If true, these processes must be something like collisional resurfacing, that has

been active since the observed Kuiper belt was put in place.

6. Additional Considerations

In this section we compare our model to other important features of the trans-Neptunian population.

6.1. The final mass of the Kuiper belt

In run A, 180 particles out of 60,000 remained permanently captured in non-resonant orbits with $a < 48$ AU. The Nice model requires that the primordial planetesimal disk was $\sim 35 M_{\oplus}$ and that roughly $\sim 25 M_{\oplus}$ remained in the disk at the time of the instability. Combining these numbers we find that run A predicts that the mass of the classical belt should be $\sim 0.07 M_{\oplus}$. In run B, we find that 360 particles are trapped, and 125 in run C. Thus, our model predicts that the classical Kuiper belt should contain between ~ 0.05 and $\sim 0.14 M_{\oplus}$. These results are of the same order as the observed mass of the Kuiper belt, which is estimated to be in the range $0.01\text{--}0.1 M_{\oplus}$ (Gladman et al. 2001; Bernstein et al. 2004), of which between 80% and 90% is in the classical population (Trujillo et al. 2001; Kavelaars et al. 2007). Thus, our model explains the mass deficit of the Kuiper belt.

Of course, to be viable, our model needs to explain not only the total mass of the belt, but also the total number of bright, detectable bodies found there. This supplies an important constraint on the original size distribution in the planetesimal disk. In fact it is obvious that, if the original size distribution was such that the bulk of the mass was carried by small bodies (meters to few kilometers in size), the captured population would not have a sufficient number of detectable objects.

Given that the trapping efficiency in the classical belt is of order 10^{-3} , our model requires that there were ~ 1000 Pluto-size bodies in the original planetesimal disk. This is in agreement with the expectations (for example see Stern 1991) that are based on the low probabilities of: 1) the capture of Triton by Neptune (for example see Agnor & Hamilton 2006), 2) the formation of the Pluto–Charon binary by an energetic collision of two large objects (Canup 2005), and 3) the existence of Pluto-size bodies (e.g. Eris) in the scattered disk². It might be possible to argue that each of these low probability events, taken individually, could occur at random even if the original number of Pluto-size objects were small. However, we strongly feel that the fact that all the three events happened almost proves that there were originally a large number of Plutos.

Because the dynamical evolution of the disk particles is independent of size, our model requires that the original size distribution in the disk was similar to that currently observed in the Kuiper belt, namely one which breaks from a steep to a shallow slope at about 50–100 km in diameter (Bernstein et al. 2004). This size distribution fits in nicely with the Nice model for two reasons. First, O’Brien et al. (2005) showed a $35 M_{\oplus}$ disk, like the one required by the Nice model, would not be significantly altered by collisions during the ~ 600 Myr that preceded the LHB if it had this size-distribution. Moreover, Charnoz & Morbidelli (2006) showed that such a disk can explain the total number of comet-size bodies in the Oort cloud and in the scattered disk.

²Independent of how it originally formed, the scattered disk represents not more than 1% of the pristine disk population (see for instance Duncan & Levison 1997).

6.2. Orbital distribution of the Plutinos

Up to now we have considered only the orbital distribution in the classical belt. However, another important diagnostic of any model is whether it can reproduce the orbital element distribution inside the major mean motion resonances with Neptune, in particular the 2:3. In fact, in contrast with all previous scenarios of Kuiper belt formation, our model does not include mean motion resonance sweeping of a cold disk of planetesimals. In all our runs, the initial location of the 2:3 MMR is beyond the outer edge of the particle disk, and thus, there is no contribution from the mechanism proposed by Malhotra (1993, 1995). Therefore, the investigation of the distribution of Plutinos can provide an important venue for comparing our model to previous scenarios.

Fig. 13 compares the e - i distribution of the Plutinos obtained in run A, against the observed distribution. When studying this figure it is important to note that the observed distribution suffers from observational biases, while the model distribution does not. Unfortunately, we cannot account for observational biases as we did for the classical belt because of the dynamics of the resonance itself. Our bias calculation assumes a uniform distribution of all orbital angles and that there is no correlation between inclination, eccentricity, and these angles. For objects in the 2:3 MMR there is a strong correlation between the argument of perihelion and the values of the eccentricity and inclination due to a strong Kozai effect (Kozai 1962; Williams & Bensen 1971; Morbidelli et al. 1995). As a result, the observed eccentricity and inclination distributions are very sensitive to exactly where in the sky the telescopes were pointed (Gladman, pers. comm.). This information is not available.

In Fig. 13 there is a good agreement between the two inclination distributions, at least by eye. The major difference seen between the two distributions in the figure is in the eccentricity distribution — the eccentricities are larger in the observations. This could be

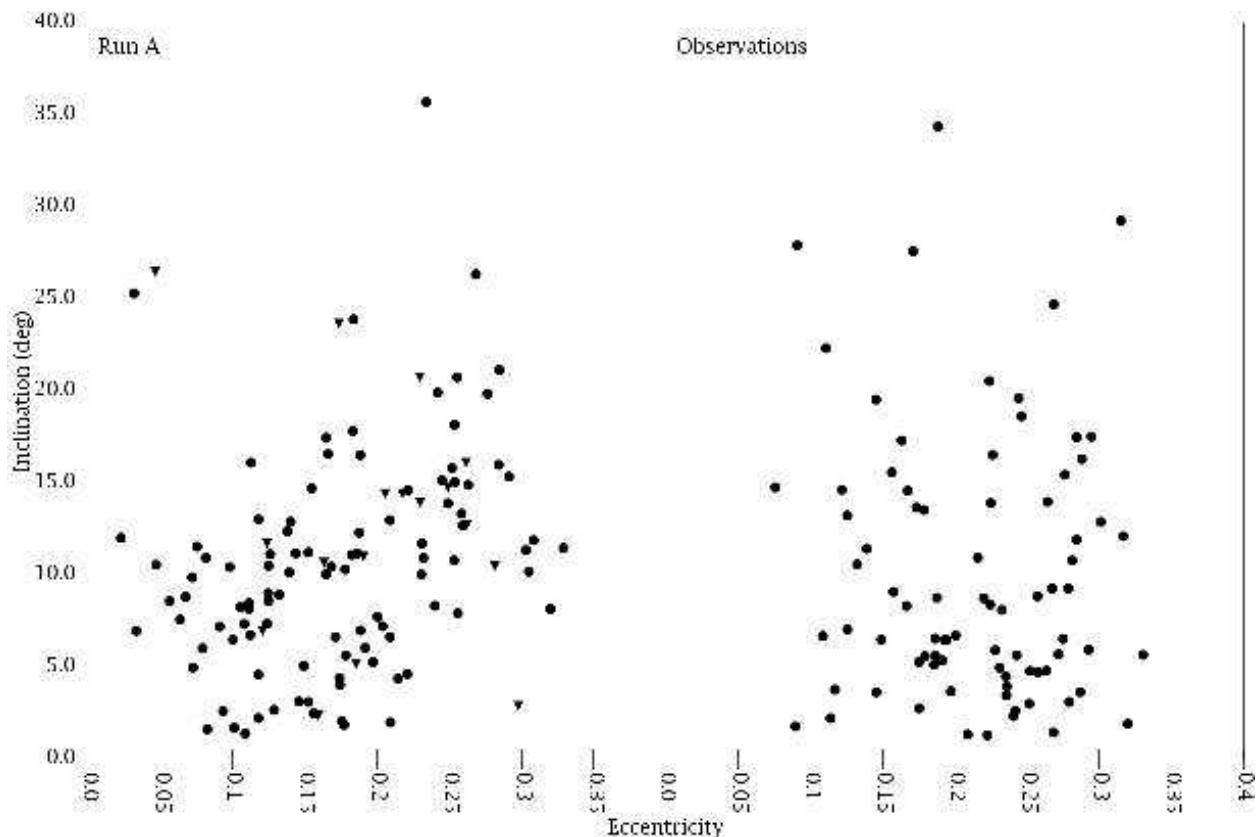


Fig. 13.— The eccentricity–inclination distribution of the Plutinos. Left panel: the result of run A; dots refer to particles from the outer disk and triangles to particles from the inner disk. Right panel: the observed distribution.

the result of the observational biases.

In the left panel of Fig. 13, the dots refer to particles captured from the outer disk and the triangles to particles from the inner disk. Outer disk particles dominate the distribution slightly. The ratio between inner disk and outer disk particles is similar to the one obtained for the hot population of the classical belt. Therefore, our model predicts that the Plutinos and the hot population should share the same physical characteristics — at least when it comes to those characteristics related to formation location. In addition, the cold population should be different. More data is needed before we can do such an analysis.

Despite some difficulties and uncertainties, the distribution of the Plutinos obtained in our model is much better than in any other previous model. In the models of Malhotra (1995) and Hahn & Malhotra (2005), the inclination distribution of the Plutinos should be similar to that of the pre-migrated planetesimal disk interior to 40 AU. Although Malhotra (1995) demonstrated that some of the bodies captured in the 2:3 resonance can acquire large inclinations (or an inclination different from its pristine one), Gomes (2000), who studied in detail the inclination excitation mechanism, concluded that these changes would not modify the inclination distribution enough to explain the observations. So, in the models by Malhotra (1995) and Hahn & Malhotra (2005), the only way to explain the fact that the Plutinos and the classical belt beyond 42 AU have different i distributions — the Plutinos lack the cold core — is if there was a sudden break in the inclination distribution of pre-migrated planetesimal disk at the current location of the 3:2 MMR. Given that there is no physical reason why this break should be near the 3:2 MMR’s current location³, this juxtaposition must be a coincidence according to these models. This seems unlikely. In Gomes (2003), the Plutinos are a mixture of bodies trapped from the scattered disk, originally formed closer to Neptune, and bodies trapped from a more distant cold disk as in Malhotra (1995). Thus, we would expect the same inclination distribution and the same correlations between physical characteristics and orbits in the Plutinos as we see in the classical belt. This is not observed.

³To be clear, the fact that the inclination distribution of the Plutinos is different from the classical belt is not discussed by Malhotra (1995) or Hahn & Malhotra (2005). The main conclusion of these works is that the resonance capture does not significantly change the inclination distribution and so the observed inclination distribution in the resonances must represent the state of the disk before the planets migrated. They do not study the excitation of the disk. The rest of this discussion is our interpretation of this result.

The fact that the Plutinos do not have a low-inclination core and that the distribution of physical properties of the Plutinos is comparable to that of the hot population are important constraints for any model. These characteristics are achieved in our model because of two essential ingredients: (i) the assumption of a truncated disk at ~ 34 AU and (ii) the fact that Neptune ‘jumps’ directly to 27–28 AU. As a result, the 2:3 MMR does not migrate through the disk, but instead jumps over it.

6.3. Mean motion resonance populations beyond 50 AU

In the final a - e distributions obtained in run A, B and C (see Figs. 6, 9, and 10), there are clearly particles trapped in mean motion resonances beyond 50 AU. This includes objects in the 4:9 (51.7 AU), 3:7 (53 AU), 2:5 (55.4 AU), and the 3:8 MMRs (57.9 AU). The 2:5 MMR has the most prominent population. This is consistent with the observed distribution in the belt (Chiang et al. 2003).

In a recent paper, Lykawka & Mukai (2006) studied the orbital distribution of objects in these resonances and pointed out that these distributions supply important constraints for any Kuiper belt formation scenario. In particular, they argue that the libration amplitude distribution can be an important diagnostic. Thus, here we compare the results of our model to the observations, concentrating, as suggested by Lykawka & Mukai, on the 2:5 MMR with Neptune. In Fig.14, we show the eccentricity, inclination, and libration amplitude of objects in this resonance. The left two panels report the results from run A, while the right two panels show the observations. The libration amplitudes for the real 2:5 librators is taken from Lykawka & Mukai (2006). Visually, there is excellent agreement between the model and the observations. (Unfortunately, for reason discussed in sect. 6.2, we cannot do a quantitative comparison) We consider this result an important accomplishment of our model.

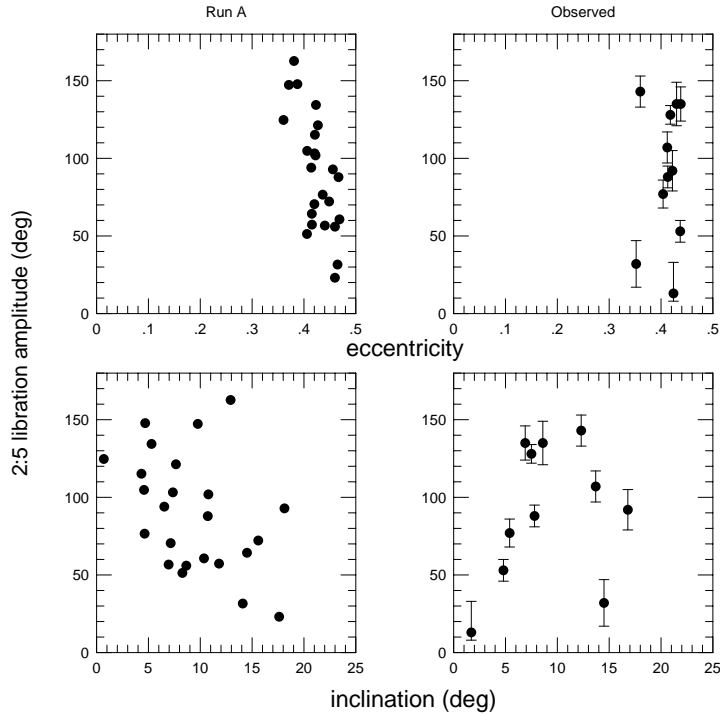


Fig. 14.— Projections of the eccentricity–inclination– libration amplitude distribution of objects in Neptune’s 2:5 MMR. The left two panels show the results from run A, while the right two panels show the observations. The libration amplitudes of the real objects is taken from Lykawka & Mukai (2006).

7. Conclusions

In this paper, we have studied the origin and orbital evolution of the Kuiper belt in the context of the Nice model for the orbital evolution of the giant planets. Recall that the Nice model explains, for the first time, the orbital architecture of the giant planets (Tsiganis et al. 2005), the origin of the late heavy bombardment in the inner solar system (Gomes et al. 2005), the existence of the Trojans of Jupiter (Morbidelli et al. 2005) and of Neptune (Tsiganis et al. 2005; Trujillo & Sheppard 2006), and the origin of at least some of the giant planet irregular satellites (Nesvorný et al. 2006).

Based on the simulations of the Nice model we presuppose that the proto-planetary disk was truncated at ~ 30 AU so that Neptune does not migrate too far (see Gomes et al. 2004). In addition, we assume that Neptune was scattered outward by Uranus to a semi-major axis between 27 and 29 AU and an eccentricity of ~ 0.3 , after which its eccentricity damped on a timescale of roughly 1 Myr. Furthermore, we assume the inclinations of the planets remained small during this evolution. Given these premises, we find that our simulations reproduce the main observed properties of the trans-Neptunian population: 1) the co-existence of resonant and non-resonant populations, 2) the peculiar a - e distribution of the classical belt, 3) the existence of an outer edge at the location of the 1:2 MMR with Neptune, 4) the bi-modal inclination distribution of the classical population, 5) the correlations between physical properties and inclination, 6) the orbital distribution of the Plutinos and the 2:5 librators, 7) the existence of the extended scattered disk, and, last but not least, 8) the mass deficit.

Our models suffer from a significant problem, however: The eccentricities are too large in our classical belt. The median eccentricity that we obtain is 0.10–0.13, whereas the observed value is 0.07. Although this problem is significant, we believe that it cannot be used as an argument against this scenario. When looking at the Kuiper belt at the level

of detail we have attempted here (which, in itself, is unprecedented), the set of planetary evolutions that are consistent with the observed structure becomes extremely narrow and we probably have not been able to pin-point it yet. This seems particularly likely given that we have only been able to perform a few simulations and held some free parameters constant (like Neptune’s initial eccentricity). It is also possible that some differences are just a statistical fluke, or some are due to missing physics in our simulations (such as stochasticity during planet migration or collisional damping). Only future models will tell.

Although when it comes to using the Kuiper belt to unravel the history of the planets the devil is in the details, we think that the list of successes of our model outweighs the problems that remain open. No other model ever reproduced the observed Kuiper belt nearly as closely as the one in this study. Indeed, only Hahn & Malhotra (2005), who studied the classical resonance sweeping scenario, have attempted the type of comparison that we presented here. They find that the list of successes of their model is much more limited. It explains the existence of resonant bodies and their eccentricity range. But it fails to explain the (e, i) distribution inside the resonances. It requires an independent and unspecified excitation mechanism to explain the (e, i) distribution in the classical belt and the existence of objects in the resonances beyond 50 AU. It cannot explain the mass deficit of the classical belt, but it has to rely on yet another mechanism (collisional grinding) for it. It cannot explain why the outer edge of the Kuiper belt is so close to the 1:2 MMR of Neptune so that it has to invoke a coincidence. So, an improbable patchwork of models is required in order to explain the Kuiper belt as a whole in the scenario.

Thus, we tentatively conclude that the structure of the Kuiper belt is an additional, substantial argument in support of the Nice model. If our conclusion is correct, and the Nice model is valid, then the Kuiper belt is the relic of the primordial massive planetesimal disk that surrounded the planets and that triggered a late instability of the outer planetary

system. This instability caused the lunar late heavy bombardment. The Kuiper belt acquired its present observed characteristics during that time, which was a seismic shake-up that totally reshaped the solar system structure.

HFL is grateful for funding from NASA’s Origins, OPR, and PGG programs. AM acknowledges funding from the french National Programme of Planetaology (PNP). R.G. is grateful to Conselho Nacional de Desenvolvimento Científico e Tecnológico for the financial support. We would also like to thank Brett Gladman for suppling us with the ability to dynamically classify our objects, and to Bill Bottke and David Nesvorný for useful discussions.

References

- Agnor, C. B., Hamilton, D. P. 2006. Neptune’s capture of its moon Triton in a binary-planet gravitational encounter. *Nature* 441, 192-194.
- Allen, R. L., Bernstein, G. M., Malhotra, R. 2001. The Edge of the Solar System. *Astrophysical Journal* 549, L241-L244.
- Allen, R. L., Bernstein, G. M., Malhotra, R. 2002. Observational Limits on a Distant Cold Kuiper Belt. *Astronomical Journal* 124, 2949-2954.
- Bernstein, G. M., Trilling, D. E., Allen, R. L., Brown, M. E., Holman, M., Malhotra, R. 2004. The Size Distribution of Trans-Neptunian Bodies. *Astronomical Journal* 128, 1364-1390.
- Brasser, R., Duncan, M. J., Levison, H. F. 2006. Embedded star clusters and the formation of the Oort Cloud. *Icarus* 184, 59-82.

- Brown, M. E. 2001. The Inclination Distribution of the Kuiper Belt. *Astronomical Journal* 121, 2804-2814.
- Canup, R. M. 2005. A Giant Impact Origin of Pluto-Charon. *Science* 307, 546-550.
- Charnoz, S., Morbidelli, A. 2006. Coupled Dynamical And Collisional Evolution Of The Oort Cloud And The Kuiper Belt. AAS/Division for Planetary Sciences Meeting Abstracts 38, #34.04.
- Chiang, E. I., Jordan, A. B., Millis, R. L., Buie, M. W., Wasserman, L. H., Elliot, J. L., Kern, S. D., Trilling, D. E., Meech, K. J., Wagner, R. M. 2003. Resonance Occupation in the Kuiper Belt: Case Examples of the 5:2 and Trojan Resonances. *Astronomical Journal* 126, 430-443.
- Doressoundiram, A., Barucci, M. A., Romon, J., Veillet, C. 2001. Multicolor Photometry of Trans-neptunian Objects. *Icarus* 154, 277-286.
- Doressoundiram, A., Barucci, M. A., Tozzi, G. P., Poulet, F., Boehnhardt, H., de Bergh, C., Peixinho, N. 2005. Spectral characteristics and modeling of the trans-neptunian object (55565) 2002 AW₁₉₇ and the Centaurs (55576) 2002 GB₁₀ and (83982) 2002 GO₉: ESO Large Program on TNOs and Centaurs. *Planetary and Space Science* 53, 1501-1509.
- Duncan, M. J., Levison, H. F., Budd, S. M. 1995. The Dynamical Structure of the Kuiper Belt. *Astronomical Journal* 110, 3073-3081.
- Duncan, M. J., Levison, H. F. 1997. A scattered comet disk and the origin of Jupiter family comets. *Science* 276, 1670-1672.
- Elliot, J. L., and 10 colleagues 2005. The Deep Ecliptic Survey: A Search for Kuiper Belt Objects and Centaurs. II. Dynamical Classification, the Kuiper Belt Plane, and the

- Core Population. *Astronomical Journal* 129, 1117-1162.
- Fernández, J. A., Morbidelli, A. 2006. The population of faint Jupiter family comets near the Earth. *Icarus* 185, 211-222.
- Gladman, B., Kavelaars, J. J., Petit, J.-M., Morbidelli, A., Holman, M. J., Loredó, T. 2001. The Structure of the Kuiper Belt: Size Distribution and Radial Extent. *Astronomical Journal* 122, 1051-1066.
- Gladman, B., Marsden, B. G., VanLaerhoven, C. 2007. Nomenclature in the Outer Solar System. *Kuiper Belt*, in press.
- Gomes, R. S. 2003. The origin of the Kuiper Belt high-inclination population. *Icarus* 161, 404-418.
- Gomes, R. S., Morbidelli, A., Levison, H. F. 2004. Planetary migration in a planetesimal disk: why did Neptune stop at 30 AU?. *Icarus* 170, 492-507.
- Gomes, R., Levison, H. F., Tsiganis, K., Morbidelli, A. 2005. Origin of the cataclysmic Late Heavy Bombardment period of the terrestrial planets. *Nature* 435, 466-469.
- Grundy, W. M., Noll, K. S., Stephens, D. C. 2005. Diverse albedos of small trans-neptunian objects. *Icarus* 176, 184-191.
- Hahn, J. M., Malhotra, R. 1999. Orbital Evolution of Planets Embedded in a Planetesimal Disk. *Astronomical Journal* 117, 3041-3053.
- Hahn, J. M., Malhotra, R. 2005. Neptune's Migration into a Stirred-Up Kuiper Belt: A Detailed Comparison of Simulations to Observations. *Astronomical Journal* 130, 2392-2414.
- Haisch, K. E., Jr., Lada, E. A., Lada, C. J. 2001. Disk Frequencies and Lifetimes in Young Clusters. *Astrophysical Journal* 553, L153-L156.

- Holman, M. J., Wisdom, J. 1993. Dynamical stability in the outer solar system and the delivery of short period comets. *Astronomical Journal* 105, 1987-1999.
- Kavelaars, J. J., Jones, L., Gladman, B., Parker, J. W., Petit, J.-M. 2007. The orbital and spatial distribution of the Kuiper belt. *Kuiper Belt*, in press.
- Kenyon, S. J., Luu, J. X. 1998. Accretion in the Early Kuiper Belt. I. Coagulation and Velocity Evolution. *Astronomical Journal* 115, 2136-2160.
- Kenyon, S. J., Luu, J. X. 1999a. Accretion in the Early Kuiper Belt. II. Fragmentation. *Astronomical Journal* 118, 1101-1119.
- Kenyon, S. J., Luu, J. X. 1999b. Accretion in the Early Outer Solar System. *Astrophysical Journal* 526, 465-470.
- Kenyon, S. J., Bromley, B. C. 2004a. Stellar encounters as the origin of distant Solar System objects in highly eccentric orbits. *Nature* 432, 598-602.
- Kenyon, S. J., Bromley, B. C. 2004b. The Size Distribution of Kuiper Belt Objects. *Astronomical Journal* 128, 1916-1926.
- Kominami, J., Tanaka, H., Ida, S. 2005. Orbital evolution and accretion of protoplanets tidally interacting with a gas disk. *Icarus* 178, 540-552.
- Kozai, Y. 1962. Secular perturbations of asteroids with high inclination and eccentricity. *Astronomical Journal* 67, 591.
- Levison, H. F., Duncan, M. J. 1994. The long-term dynamical behavior of short-period comets. *Icarus* 108, 18-36.
- Levison, H. F., Duncan, M. J. 1997. From the Kuiper Belt to Jupiter-Family Comets: The Spatial Distribution of Ecliptic Comets. *Icarus* 127, 13-32.

- Levison, H. F., Stern, S. A. 2001. On the Size Dependence of the Inclination Distribution of the Main Kuiper Belt. *Astronomical Journal* 121, 1730-173
- Levison, H. F., Stewart, G. R. 2001. Remarks on Modeling the Formation of Uranus and Neptune. *Icarus* 153, 224-228.
- Levison, H. F., Morbidelli, A. 2003. The formation of the Kuiper belt by the outward transport of bodies during Neptune's migration. *Nature* 426, 419-421.
- Lubow, S. H., Seibert, M., Artymowicz, P. 1999. Disk Accretion onto High-Mass Planets. *Astrophysical Journal* 526, 1001-1012.
- Lykawka, P. S., Mukai, T. 2006. Evidence for an excited Kuiper belt of 50AU radius in the first Myr of Solar system history. *Icarus*, in press.
- Malhotra, R. 1993. The Origin of Pluto's Peculiar Orbit. *Nature* 365, 819.
- Malhotra, R. 1995. The Origin of Pluto's Orbit: Implications for the Solar System Beyond Neptune. *Astronomical Journal* 110, 420.
- Masset, F., Snellgrove, M. 2001. Reversing type II migration: resonance trapping of a lighter giant protoplanet. *Monthly Notices of the Royal Astronomical Society* 320, L55-L59.
- Morbidelli, A., Thomas, F., Moons, M. 1995. The resonant structure of the Kuiper belt and the dynamics of the first five trans-Neptunian objects. *Icarus* 118, 322.
- Morbidelli, A. 2002. Modern Integrations of Solar System Dynamics. *Annual Review of Earth and Planetary Sciences* 30, 89-112.
- Morbidelli, A., Emel'yanenko, V. V., Levison, H. F. 2004. Origin and orbital distribution of the trans-Neptunian scattered disc. *Monthly Notices of the Royal Astronomical Society* 355, 935-940.

- Morbidelli, A., Brown, M. E. 2004. The kuiper belt and the primordial evolution of the solar system. *Comets II* 175-191.
- Morbidelli, A., Levison, H. F. 2004. Scenarios for the Origin of the Orbits of the Trans-Neptunian Objects 2000 CR₁₀₅ and 2003 VB₁₂ (Sedna). *Astronomical Journal* 128, 2564-2576.
- Morbidelli, A., Levison, H. F., Tsiganis, K., Gomes, R. 2005. Chaotic capture of Jupiter's Trojan asteroids in the early Solar System. *Nature* 435, 462-465.
- Morbidelli, A., Crida, A. 2007. The dynamics of Jupiter and Saturn in the gaseous proto-planetary disk. *Icarus*, submitted.
- Murray-Clay, R. A., Chiang, E. I. 2006. Brownian Motion in Planetary Migration. *Astrophysical Journal* 651, 1194-1208.
- Nesvorný, D., Vokrouhlický, D., Morbidelli, A. 2007. Capture of Irregular Satellites during Planetary Encounters. *Astronomical Journal* 133, 1962-1976.
- O'Brien, D. P., Morbidelli, A., Bottke, W. F. 2005. Collisional Evolution of the Primordial Trans-Neptunian Disk: Implications for Planetary Migration and the Current Size Distribution of TNOs. *Bulletin of the American Astronomical Society* 37, 676.
- Pollack, J. B., Hubickyj, O., Bodenheimer, P., Lissauer, J. J., Podolak, M., Greenzweig, Y. 1996. Formation of the Giant Planets by Concurrent Accretion of Solids and Gas. *Icarus* 124, 62-85.
- Press, W., Teukolsky, S.A., Vetterling, W.T., Flannery, B.P. 1992. *Numerical Recipes in Fortran. The art of scientific computing*, 2nd edition. Cambridge University Press.
- Safronov, V.S. 1969. 'Evolution of the Protoplanetary Cloud and the Formation of the Earth and Planets. Nauka Press.

- Sheppard, S. S., Trujillo, C. A. 2006. A Thick Cloud of Neptune Trojans and Their Colors. *Science* 313, 511-514.
- Stern, S. A. 1991. On the number of planets in the outer solar system - Evidence of a substantial population of 1000-km bodies. *Icarus* 90, 271-281.
- Stern, S. A. 1996. On the Collisional Environment, Accretion Time Scales, and Architecture of the Massive, Primordial Kuiper Belt.. *Astronomical Journal* 112, 1203.
- Stern, S. A., Colwell, J. E. 1997a. Accretion in the Edgeworth-Kuiper Belt: Forming 100-1000 KM Radius Bodies at 30 AU and Beyond.. *Astronomical Journal* 114, 841.
- Stern, S. A., Colwell, J. E. 1997b. Collisional Erosion in the Primordial Edgeworth-Kuiper Belt and the Generation of the 30-50 AU Kuiper Gap. *Astrophysical Journal* 490, 879.
- Tegler, S. C., Romanishin, W. 2000. Extremely red Kuiper-belt objects in near-circular orbits beyond 40 AU. *Nature* 407, 979-981.
- Tera F, Papanastassiou, D.A., Wasserburg, G.J. 1974. Isotopic Evidence for a terminal lunar cataclysm. *Earth Planet Sci. Lett.* 22, 1-21.
- Thommes, E. W., Duncan, M. J., Levison, H. F. 2003. Oligarchic growth of giant planets. *Icarus* 161, 431-455.
- Trujillo, C. A., Brown, M. E. 2001. The Radial Distribution of the Kuiper Belt. *Astrophysical Journal* 554, L95-L98.
- Trujillo, C. A., Jewitt, D. C., Luu, J. X. 2001. Properties of the Trans-Neptunian Belt: Statistics from the Canada-France-Hawaii Telescope Survey. *Astronomical Journal* 122, 457-473.
- Trujillo, C. A., Brown, M. E. 2002. A Correlation between Inclination and Color in the Classical Kuiper Belt. *Astrophysical Journal* 566, L125-L128.

Tsiganis, K., Gomes, R., Morbidelli, A., Levison, H. F. 2005. Origin of the orbital architecture of the giant planets of the Solar System. *Nature* 435, 459-461.

Wisdom, J., Holman, M. 1991. Symplectic maps for the n-body problem. *Astronomical Journal* 102, 1528-1538.